~~Revealing the Driving Factors of Water Balance in Lake Balkhash Through Integrated Attribution Modeling~~

Disentangling the Key Drivers of Water Balance in Central Asia's Lake Balkhash: A Relative Contribution Assessment

Ruibiao Yang[1,2,3], Jinglu Wu[1,2], Guojing Gan[1,2], Ru Guo[1,2,3]

[1]State Key Laboratory of Lake Science and Environment, Nanjing Institute of Geography and Limnology, Chinese Academy of Science, Nanjing 210008, China
[2]University of Chinese Academy of Sciences, Beijing 100049, China
[3]College of Nanjing, University of Chinese Academy of Sciences, Nanjing 211135, China

Correspondence to: Jinglu Wu (w.jinglu@niglas.ac.cn)

Abstract~~.~~: Lake Balkhash, a vital endorheic system in Central Asia, faces increasing hydrological uncertainty driven by the interplay of climate change and anthropogenic disturbances. Disentangling the individual contributions of these concurrent drivers is essential for sustainable basin management but remains methodologically challenging due to data scarcity and complex feedback mechanisms. This study introduces the Hydrological Analysis and Disentanglement Framework (HADF) to strictly quantify the drivers of the lake's centennial water balance (1931–2024). By integrating a hybrid hydrological model—coupling SEGSWAT+ with machine learning error correction—with the Budyko framework, we reconstructed historical naturalized and actual inflow with high fidelity (KGE > 0.75) and explicitly linked catchment-scale drivers to lake storage dynamics. Our results reveal a system defined by substantial, opposing forces. During the intensive intervention period (1970–1990), human water withdrawal was the dominant driver of inflow decline, reducing runoff by 9.21 km³/yr and effectively masking a significant climate-driven wetting trend (+6.13 km³/yr). In the recent period (1991–2024), the lake entered a state of "masked vulnerability": a large climate-driven potential for recovery (+10.80 km³/yr), fueled by increased precipitation and glacial melt, was almost entirely neutralized by sustained human consumption (-11.36 km³/yr). Consequently, the recent stability of Lake Balkhash is not a sign of intrinsic resilience but a fragile equilibrium supported by a transient climatic subsidy. Future projections under Shared Socioeconomic Pathways (SSPs) indicate that as this climatic benefit wanes, the system risks a rapid decline, with water levels potentially dropping 2.5–4.0 meters by 2100. These findings underscore the urgency of decoupling water allocation policies from temporary climatic bonuses to prevent irreversible ecological degradation.

~~Understanding the impacts of climate change and human activities on large endorheic lakes is crucial for sustainable water management, yet quantitative attribution remains a significant challenge. This study introduces the Hydrological Attribution and Analysis Framework (HAAF), a novel three-stage methodology, to provide a comprehensive explanation for the nearly-centennial (1931–2024) water balance dynamics of Lake Balkhash. The HAAF first establishes a high-fidelity hydrological reconstruction using a Physics-Informed Machine Learning (PIML) model, then employs the Budyko framework to attribute~~

Formatted: Font: (Default) +Headings (Times New Roman)

Formatted: Font: (Default) +Headings (Times New Roman), Not Bold

Formatted: Font: (Default) +Headings (Times New Roman)

runoff changes, and finally links these catchment-scale drivers to the lake's terminal water balance. Our results confirm the robustness of the PIML model in simulating historical runoff (KGE > 0.75). The attribution analysis then reveals a complex interplay of competing forces. During the intensive intervention period (1970-1990), a substantial human-induced runoff reduction of -9.21 km³ completely masked a significant climate-driven wetting potential (+6.13 km³), triggering the lake's sharp decline. In the recent period (1991-2024), the basin's hydrology has been governed by a fragile stalemate in which a massive, climate-driven potential for increased runoff (+10.80 km³) was almost entirely neutralized by the persistent negative impact of human water use (-11.36 km³). At the lake level, this translated into an apparent stability sustained only by a favorable climatic subsidy. Future projections under various climate scenarios indicate that this climatic buffer is transient and unlikely to persist, exposing the lake to a high risk of rapid decline. We conclude that the recent stability of Lake Balkhash is not a sign of systemic recovery but a "masked vulnerability." This highlights the urgent need for transboundary water management strategies that account for these underlying, competing drivers.

1 Introduction

Endorheic lakes in arid and semi-arid regions are widely recognized as sensitive indicators of hydroclimatic change (Zhang et al., 2021). The water level and ecological health of these lakes are governed by a delicate balance between water inputs from their catchments and evaporative losses. Today, this balance is increasingly under pressure from two primary forces: global climate change, which alters precipitation patterns, temperature, and cryospheric contributions, and direct human activities, such as water withdrawal for agriculture and reservoir regulation However, decreasing water storage has become a widespread issue for these lakes, posing a significant threat to their ecological health (Li et al., 2025). This decline is primarily driven by two concurrent forces: global climate change, which alters precipitation patterns and cryospheric contributions, and direct human activities, such as water withdrawal for agriculture and reservoir regulation (Immerzeel and Bierkens, 2012; Li et al., 2016; Mandal and Chanda, 2023). For instance, the Aral Sea has substantiallydramatically shrunk due to irrigation diversions, while Lake Urmia faces similar threats from water abstraction and drought. These examples underscore the global relevance of understanding water balance dynamics in closed basins, where water cycles are tightly coupled with climate and anthropogenic activities. Disentangling the individual impacts of these concurrent drivers is a fundamental challenge in hydrology and Earth system science. A robust quantitative assessment of these driving forces attribution is not only crucial for understanding past hydrological dynamics but also essential for developing sustainable water management strategies and predicting the future trajectory of these vital ecosystems.

Lake Balkhash exemplifies these interactions, with its transboundary basin shared between Kazakhstan and China, primarily fed by the Ili River from glacial and snow melt in the Tianshan Mountains (Duan et al., 2020). Historical fluctuations include sharp declines in the 20th century, followed by relative stability, amid accelerating warming and human water use (Duan et al., 2021). As an endorheic lake, Lake Balkhash has no outlet, and all its incoming runoffinflow is ultimately lost to evaporation.

Formatted: Font: (Default) +Headings (Times New Roman), Font color: Auto

Formatted: Font: (Default) +Headings (Times New Roman)

Formatted: Font: (Default) +Headings (Times New Roman)

Formatted: Font: (Default) +Headings (Times New Roman)

Formatted: Font: (Default) +Headings (Times New Roman)

Formatted: Font: (Default) +Headings (Times New Roman)

Formatted: Font: (Default) +Headings (Times New Roman)

Formatted: Font: (Default) +Headings (Times New Roman)

Formatted: Font: (Default) +Headings (Times New Roman), Font color: Auto

Formatted: Font: (Default) +Headings (Times New Roman)

Formatted: Font: (Default) +Headings (Times New Roman)

Formatted: Font: (Default) +Headings (Times New Roman)

Its primary source region is experiencing a warming rate significantly higher than the global average, accelerating glacial melt (Jin et al., 2024). ~~While this melt initially boosts lake inflow in the short term, it signals a long-term depletion of solid water reserves.~~While increasing glacier melt can temporarily raise inflow, it leads to the irreversible depletion of solid water reserves. This continuous loss of ice storage implies that the current meltwater increase is transient, and future water availability will be threatened as the glacial volume diminishes. This shifting composition of water sources heightens the lake's sensitivity to climatic fluctuations, underscoring the significant~~profound~~ impact of climate change on its hydrology. Concurrently, anthropogenic activities, particularly water consumption in the lower Ili River basin, have been identified as a key driver of the lake's water level decline in the latter half of the 20th century, raising~~sparking~~ significant concerns regarding transboundary water management and sustainability (Cai et al., 2014).

Reduced inflow not only directly lowers the water level of Lake Balkhash but also triggers a cascade of ecological consequences, such as delta ecosystem degradation (Starodubtsev and Truskavetskiy, 2011), increased lake salinity (Shen et al., 2021), and the degradation~~destruction~~ of aquatic habitats (Li et al., 2021). Although previous research has identified climate and human activities as the primary drivers of streamflow~~runoff~~ change and attempted to estimate~~quantify~~ their relative contributions using distributed hydrological models (Gan et al., 2022; Wang et al., 2024; Yu et al., 2025)~~, these studies often fail to integrate their findings with the lake's terminal water balance, hindering a comprehensive explanation. The region's scarcity of long-term, high-quality observational data on inflow, especially for naturalized flow (i.e., runoff unaltered by human interference), poses a significant challenge. For the same reason, simulations using traditional hydrological models or machine learning (ML) methods in this area are subject to high uncertainty. These limitations impede a clear differentiation and comparison of the impacts of climate change and human activities across different periods, leaving a critical knowledge gap regarding the dominant factors governing the lake's water fluctuations.~~ , two critical gaps remain. First, a methodological gap exists in handling the region's data scarcity and high uncertainty. While limited observations pose a challenge for all modeling approaches, traditional physics-based models are particularly vulnerable to parameter equifinality and structural errors when calibration data is sparse (Yang et al., 2022). Conversely, pure machine learning (ML) models require extensive datasets to learn physical laws and lack interpretability (Mohammadi, 2021). The specific advantage of the hybrid approach lies in mitigating this 'uncertainty vs. data scarcity' trade-off. By using a physics-based model to simulate the fundamental hydrological processes and then employing ML solely to learn the residuals, this approach enforces physical constraints while effectively correcting the structural biases of the physical model, improving accuracy beyond what traditional calibration can achieve with limited data. Second, existing studies typically focus on decomposing streamflow changes at the catchment outlet but fail to explicitly link these catchment-scale drivers to the lake water storage volume and water level. While studies like (Yu et al.~~,~~ (2025) quantify inflow reduction, they often stop at the river mouth. This disconnect prevents a direct quantitative explanation of how specific upstream drivers—such as the exact volume of glacial melt versus human withdrawals—translate into the observed vertical fluctuations of the lake itself, which is the ultimate metric of ecological health.

Formatted: Font: (Default) +Headings (Times New Roman)
Formatted: Font: (Default) +Headings (Times New Roman)
Formatted: Font: (Default) +Headings (Times New Roman)
Formatted: Font: (Default) +Headings (Times New Roman)
Formatted: Font: (Default) +Headings (Times New Roman)
Formatted: Font: (Default) +Headings (Times New Roman)
Formatted: Font: (Default) +Headings (Times New Roman)
Formatted: Font: (Default) +Headings (Times New Roman)
Formatted: Font: (Default) +Headings (Times New Roman), Font color: Auto
Formatted: Font: (Default) +Headings (Times New Roman)
Formatted: Font: (Default) +Headings (Times New Roman)
Formatted: Font: (Default) +Headings (Times New Roman)
Formatted: Font: (Default) +Headings (Times New Roman)
Formatted: Font: (Default) +Headings (Times New Roman)
Formatted: Font: (Default) +Headings (Times New Roman)
Formatted: Font: (Default) +Headings (Times New Roman)

To address these existing gaps, this study introduces and implements the Hydrological Analysis and DisentanglementAttribution and Analysis Framework (HAAFHADF).). This integrated methodology is designed to rigorously distinguish the drivers of hydrological change and project future vulnerabilities. The study is structured around three core objectives: a methodology designed to rigorously distinguish the drivers of hydrological change. The strength of HAAF lies in its structured approach, which first employs a PIML model for high-fidelity hydrological reconstruction to generate robust long-term interannual runoff time series. It then utilizes the Budyko framework for quantitative driver attribution, separating climatic from anthropogenic impacts on runoff. Finally, the framework provides a system-level impact linkage by connecting these attributed catchment-scale changes directly to the lake's water balance dynamics. This integrated workflow allows for a complete diagnosis from cause to effect, thereby offering a perspective on studying the water balance of lakes in arid regions, comparable to studies on other lakes where similar attribution challenges persist.

The main objective of this paper is to provide a comprehensive quantitative explanation for the centennial dynamics of Lake Balkhash's water volume by applying the HAAF methodology. To achieve this, our study is structured around the three core stages of the HAAF framework:

(1) Reconstructing high-accuracy inflow time series (1931-2024) using a hybrid model. This hybrid architecture runs a physics-based model to capture governing hydrological processes and then utilizes an ML algorithm to learn and correct the residuals. This strategy effectively mitigates the structural errors of the physical model while enforcing physical plausibility, offering a robust solution for hydrological reconstruction in data-scarce arid basins. Reconstructing the annual naturalized and human-impacted runoff into Lake Balkhash for the past century (1931-2024), employing the PIML model as the high-fidelity reconstruction engine.

(2) Quantitatively separating the relative contributions of climate change and direct human activities to the observed inflowrunoff variationschanges across three distinct historical periods, employingusing the Budyko framework for attribution.

(3) Elucidating how these attributed changes in water inputs have governed the historical water storage fluctuations of Lake Balkhash by linking them through a lake water balance equation. Providing a system-level assessment by linking these catchment drivers directly to the lake's water storage dynamics and, for the first time in this context, projecting future lake level trajectories under various Shared Socioeconomic Pathways (SSPs). This final step allows us to assess whether the lake's recent stability is sustainable or if it masks an underlying vulnerability to future climate and anthropogenic pressures.

Formatted: Font: (Default) +Headings (Times New Roman), Font color: Auto

2 Materials and Methods

2.1 Study Area and Historical Periodization

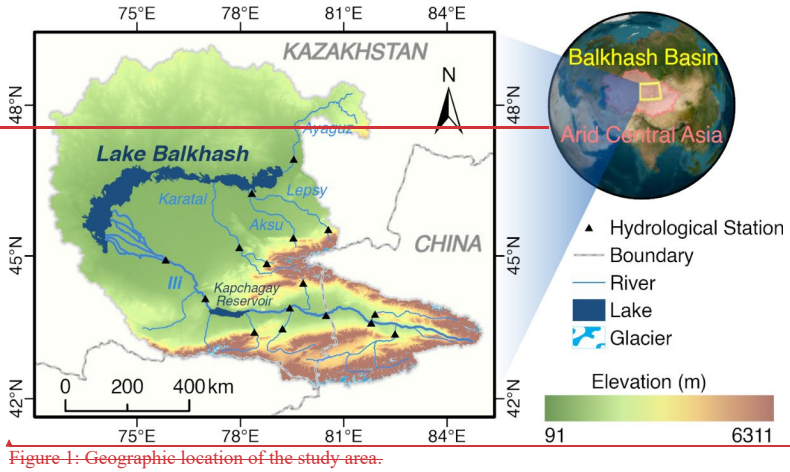

~~Figure 1: Geographic location of the study area.~~

Lake Balkhash, one of the largest endorheic lakes in the arid region of Central Asia, is situated in southeastern Kazakhstan (Duan et al., 2020). It covers an area of approximately 16,400 km², has an average depth of 5.8 meters, and exhibits **distinct**~~pronounced~~ differences in water quality between its western (freshwater) and eastern (saline) sections (Shen et al., 2021). The lake receives inflow from five primary rivers, predominantly the Ili River, which accounts for over 70% of the total inflow (Liu et al., 2024). Other significant tributaries include the Karatal, Aksu, Lepsy, and Ayaguz rivers, originating from the Tien Shan and Dzungarian Alatau ~~mountains~~Mountains. The Lake Balkhash basin encompasses a total area of approximately 413,000 km² and features an elevation range from 60 to 6,000 m (Fig~~.~~ 1). The basin is characterized by a typical temperate continental arid climate with high spatial heterogeneity. The annual spatial and seasonal distribution of precipitation reveals a stark contrast between the upstream and downstream regions. The mountainous upper reaches receive significantly higher precipitation, averaging 725 mm/year, compared to the arid plains and lake surfaces, which average only 235 mm/year (Appendix Fig. A1a)~~(Cao et al., 2022)~~. Precipitation exhibits strong seasonality, with approximately 71.2% of the annual total occurring during the spring and summer months (Appendix Fig. A1b). The high-altitude regions host widespread glaciers and seasonal snowpack, serving as critical water towers for the basin. Observed climatic changes from 1931 to 2024 indicate a pronounced warming trend, particularly in the upstream mountain ranges, with a significant temperature increase of 0.30 °C/decade and a precipitation increase of 1.11 mm/decade (Appendix Fig. A1c). This warming has accelerated in recent decades, reaching a rate of 0.47 °C/decade, further intensifying glacier melt and shifting the timing of peak runoff (Zhan et al., 2025). Furthermore, precipitation patterns are becoming increasingly variable. Under future climate scenarios, the region is

Formatted: Font: (Default) +Headings (Times New Roman), Font color: Auto

Formatted: Font: (Default) +Headings (Times New Roman)

Formatted: Font: (Default) +Headings (Times New Roman)

Formatted: Font: (Default) +Headings (Times New Roman)

Formatted: Font: (Default) +Headings (Times New Roman)

Formatted: Font: (Default) +Headings (Times New Roman)

Formatted: Font: (Default) +Headings (Times New Roman)

Formatted: Font: (Default) +Headings (Times New Roman)

Formatted: Font: (Default) +Headings (Times New Roman)

Formatted: Font: (Default) +Headings (Times New Roman)

Formatted: Font: (Default) +Headings (Times New Roman)

Formatted: Font: (Default) +Headings (Times New Roman), (Asian) +Body Asian (宋体), (Asian) Chinese (Simplified, Mainland China)

projected to experience continued warming and altered precipitation regimes, which poses additional uncertainties for the basin's water balance (Liu et al., 2024). ~~The mountainous upper reaches of the river are an area of widespread glaciers and seasonal snowpack, and these ice/snowmelt waters have traditionally been one of the main sources of water for Lake Balkhash. The entire basin is deep within the Eurasian continent, with a typical temperate continental arid climate, sparse and uneven spatial distribution of precipitation - the mountainous areas receive significantly more precipitation than the plains and lakes (Cao et al., 2022).~~

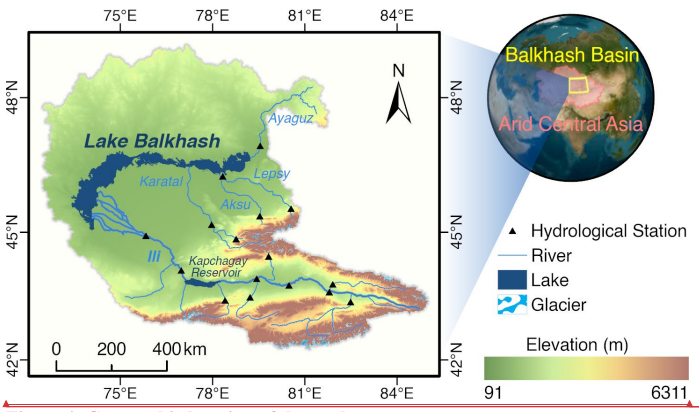

Figure 1. Geographic location of the study area.

The historical interannual water levels of Lake Balkhash are shown on Fig. 2. The hydrological history of this lake ~~Lake Balkhash~~ is marked by critical significant transitions ~~turning points~~ that have reshaped its ecosystem, influenced by both natural variability and human activities. During the 1970s and 1980s, the lake underwent a severe ecological crisis, principally driven by the impoundment of the Kapchagay Reservoir on its main tributary, the Ili River (Yu et al., 2025). This event triggered a rapid ~~sharp~~ decline in the lake's water level, a corresponding rise in salinity, and significant biodiversity loss. Following the dissolution of the Soviet Union in 1991, while direct reservoir impoundment pressures lessened, subsequent political and economic transitions ~~shifts~~ introduced new complexities, intensifying transboundary water conflicts and altering regional water management paradigms (Jia et al., 2020). In light of these pivotal events, we have structured our investigation by dividing the entire study period (1931-2024) into three distinct periods based on the 1970 and 1991 milestones to facilitate a dynamic driver ~~attribution~~ analysis. This segmentation aligns with previous studies that have validated its reasonableness for capturing shifts in hydrological drivers (Wang et al., 2024). A summary of these periods is presented in Table 1.

Formatted: Font: (Default) +Headings (Times New Roman)
Formatted: Font: (Default) +Headings (Times New Roman)
Formatted: Font: (Default) +Headings (Times New Roman)
Formatted: Font: (Default) +Headings (Times New Roman), (Asian) Chinese (Simplified, Mainland China)
Formatted: Font: (Default) +Headings (Times New Roman)
Formatted: Font: (Default) +Headings (Times New Roman), 10 pt
Formatted: Font: (Default) +Headings (Times New Roman), English (United Kingdom)
Formatted: Caption
Formatted: Font: (Default) +Headings (Times New Roman)
Formatted: Font: (Default) +Headings (Times New Roman)
Formatted: Font: (Default) +Headings (Times New Roman)
Formatted: Font: (Default) +Headings (Times New Roman)
Formatted: Font: (Default) +Headings (Times New Roman)
Formatted: Font: (Default) +Headings (Times New Roman), Font color: Auto
Formatted: Font: (Default) +Headings (Times New Roman)
Formatted: Font: (Default) +Headings (Times New Roman)
Formatted: Font: (Default) +Headings (Times New Roman), English (United States)

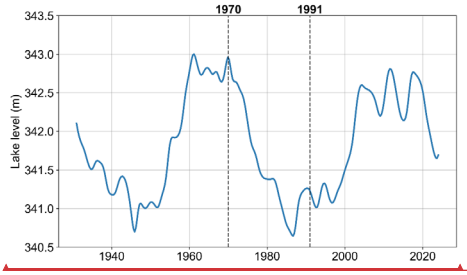

Figure 2. Water Level of Lake Balkhash, 1931–2024 (Water levels from 1901 to 2015 are based on actual observational data, while those from 2016 to 2024 are derived from the G-REALM dataset. The latter was calibrated against observed data from 2001 to 2015. Specific sources are detailed in the following subsection)

Table 1. Summary of the three defined historical periods

Period	Time Frame	Designation	Key Characteristics
P1	1931-1969	Reference Period	Limited direct hydrological intervention, with water availability primarily governed by natural climate variability.
P2	1970-1990	Intensive Intervention Period	Dominated by substantial~~intense~~ human interference, where major hydrological engineering significantly~~fundamentally~~ altered the regional water balance.
P3	1991-2024	Compounded Pressures Period	Defined by the combined effects of stabilized engineering impacts, post-Soviet shifts in water management policy, and accelerating climate change.

2.2 Datasets

~~This study employed a diverse range of datasets to support the hydrological modeling and analysis of hydro-climatic changes. These datasets include a Digital Elevation Model (DEM), soil properties, land use/land cover (LULC) maps, glacier inventories, glacier elevation changes, meteorological forcings, and observed streamflow data. A summary of these datasets is presented in Table 2, including key variables, spatial and temporal resolutions, coverage periods, and access links for reproducibility.~~This study employed a diverse range of datasets to support the hydrological modeling and analysis of hydro-climatic changes. These datasets include a Digital Elevation Model (DEM), soil properties, land use/land cover (LULC) maps, glacier inventories, glacier elevation changes, meteorological forcings, and observed streamflow data. A summary of these datasets is presented in Table 2, including key variables, spatial and temporal resolutions, coverage periods, and data sources to ensure the reproducibility of the results.

Table 2~~:~~. Summary of datasets used in this study

Formatted: Font: (Default) +Headings (Times New Roman), 10 pt
Formatted: Font: (Default) +Headings (Times New Roman), 10 pt
Formatted: Font: (Default) +Headings (Times New Roman), (Asian) +Body Asian (宋体)
Formatted: Normal
Formatted: Font: (Default) +Headings (Times New Roman), 10 pt
Formatted: Font: (Default) +Headings (Times New Roman)
Formatted: Font: (Default) +Headings (Times New Roman)
Formatted: Font: (Default) +Headings (Times New Roman)
Formatted: Font: (Default) +Headings (Times New Roman)
Formatted: Font: (Default) +Headings (Times New Roman)
Formatted: Font: (Default) +Headings (Times New Roman), English (United Kingdom)
Formatted: Font: (Default) +Headings (Times New Roman), 10 pt

Dataset	Key Variables	Spatial Resolution	Temporal Coverage	Source (Reference)
Copernicus GLO-90 DEM	Elevation	90 m	Static	European Space Agency (2019)OpenTopography
DSOLMap	Bulk density, hydraulic conductivity, available water capacity	250 m	Static	WateriTech(Lopez-Ballesteros et al., (2023)
GLC_FCS30D	Land cover classes (35 subcategories)	30 m	1985–2022	ZenodoGoogle Earth Engine(Zhang et al., 2024)
Randolph Glacier Inventory (RGI v7.0)	Glacier outlines, attributes	Vector	~2000 snapshot Target year: 2000 (varies by region)	GLIMSRGI Consortium (2023)
SWORD v15	River reaches, nodes, hydrological networks, lake boundaries	~10 km reaches, 200 m nodes	Static	Zenodo(Altenau et al. ,(2021)
Glacier mass lossHugonnet et al. (2021)	Glacier elevation change rates (dh/dt)	100 m	2000–2019	Original publication(Hugonnet et al., (2021)
CRU JRA v2.53.0	Temperature, precipitation, wind speed, vapor pressure, etc.	0.5° (downscaled to 0.05°)	1901–2024 (daily)	CEDA Archive, Harris (2024)
TerraClimate	Max/min temperature, precipitation, solar radiation, vapor pressure deficit	1/24°	1958–present—2024 (monthly)	Climatology Lab(Abatzoglou et al., (2018)
NEX-GDDP-CMIP6	Daily temperature (max/min), precipitation	0.25°	2015–2100 (Daily)	Thrasher et al. (2022)
ObservationsObserved Streamflow	Discharge (daily/monthly), water level	Point	Varies (1931–2024) (monthly)	NCDC (2024); Duan et al. (2020)National Cryosphere Desert Data Center

The Digital Elevation Model utilized was the Copernicus GLO-90 DEM, which provides elevation data at a spatial resolution of 90 meters and is accessible via OpenTopography. Soil hydraulic parameters (e.g., bulk density, hydraulic conductivity, available water capacity) were derived from DSOLMapThe Digital Elevation Model used was the Copernicus GLO-90 DEM, which provides elevation data at a spatial resolution of 90 meters and is accessible via OpenTopography. Soil hydraulic parameters (e.g., bulk density, hydraulic conductivity, available water capacity) were derived from DSOLMap (Lopez-Ballesteros et al., 2023). a 250m-resolution dataset available through WateriTech. For Land Use/Land Cover, we employed the GLC_FCS30D dataseta 250m-resolution dataset available through WateriTech. For Land Use/Land Cover, we used the GLC_FCS30D dataset (Zhang et al., 2024), (Zhang et al., 2024). This dataset offers the highest available resolution (30m) for a global, long-term LULC time series, covering the period 1985–2022 with 35 land-cover subcategories, and is available on the Zenodo platform. Glacier outlines and attributes were obtained from the Randolph Glacier Inventory v7.0 (RGI), provided by the Global Land Ice Measurements from Space (GLIMS) initiative. Hydrological networks and lake boundaries were delineated using the Surface Water and Ocean Topography mission river database (SWORD) v15. Based on a 30m DEM, this

Formatted: Font: (Default) +Headings (Times New Roman)
Formatted: Font: (Default) +Headings (Times New Roman)
Formatted: Font: (Default) +Headings (Times New Roman)
Formatted: Font: (Default) +Headings (Times New Roman)
Formatted: Font: (Default) +Headings (Times New Roman)
Formatted: Font: (Default) +Headings (Times New Roman)
Formatted: Font: (Default) +Headings (Times New Roman)
Formatted: Font: (Default) +Headings (Times New Roman)
Formatted: Font: (Default) +Headings (Times New Roman)
Formatted: Font: (Default) +Headings (Times New Roman)
Formatted: Font: (Default) +Headings (Times New Roman)
Formatted: Font: (Default) +Headings (Times New Roman)
Formatted: Font: (Default) +Headings (Times New Roman)
Formatted: Font: (Default) +Headings (Times New Roman), Portuguese (Brazil)
Formatted: Font: (Default) +Headings (Times New Roman)
Formatted: Font: (Default) +Headings (Times New Roman)
Formatted: Font: (Default) +Headings (Times New Roman), Portuguese (Brazil)
Formatted: Font: (Default) +Headings (Times New Roman), Portuguese (Brazil)
Formatted: Font: (Default) +Headings (Times New Roman)
Formatted: Font: (Default) +Headings (Times New Roman)
Formatted: Font: (Default) +Headings (Times New Roman), Portuguese (Brazil)
Formatted: Font: (Default) +Headings (Times New Roman)
Formatted: Font: (Default) +Headings (Times New Roman), English (United States)
Formatted: Font: (Default) +Headings (Times New Roman)
Formatted: Font: (Default) +Headings (Times New Roman)
Formatted: Indent: First line: 0 ch
Formatted: Font: (Default) +Headings (Times New Roman)
Formatted: Font: (Default) +Headings (Times New Roman)
Formatted: Font: (Default) +Headings (Times New Roman)
Formatted: Font: (Default) +Headings (Times New Roman)
Formatted: Font: (Default) +Headings (Times New Roman)

dataset has demonstrated superior accuracy in river network extraction compared to the widely used HydroSHEDS datasetwhich offers the highest available resolution (30m) for a global, long-term LULC time series covering 1985–2022 with 35 land-cover subcategories, and is available on the Zenodo platform. Glacier outlines and attributes were obtained from the Randolph Glacier Inventory v7.0 (RGI), provided by the Global Land Ice Measurements from Space (GLIMS) initiative. Hydrological networks and lake boundaries were delineated using the Surface Water and Ocean Topography mission river database (SWORD) v15, which is based on a 30m DEM and has demonstrated superior accuracy compared to the widely used HydroSHEDS dataset (Altenau et al., 2021). Glacier elevation change data from the study by Hugonnet et al. (2021) were used to calibrate glacier melt parameters.were used for calibrating glacier melt parameters. For historical climate forcing, we primarily utilized the CRU JRA v3.0 dataset. This dataset provides daily meteorological variables (e.g., temperature, precipitation, wind speed, vapor pressure) at a 0.5° spatial resolution from 1901 to 2024, representing the longest daily historical climate forcing dataset currently available. It is accessible through the CEDA Archive and is derived from the CRU TS dataset, whose reliability in Central Asia, particularly post-1930, has been confirmed by numerous studiesFor historical climate forcing data, we primarily utilized the CRU JRA v2.5 dataset (an update to the originally referenced v3.0 for consistency with recent releases), which provides daily meteorological variables (e.g., temperature, precipitation, wind speed, vapor pressure) at a 0.5° spatial resolution from 1901 to 2024, making it the longest daily historical climate forcing dataset currently available. It is accessible through the CEDA Archive. This dataset is derived from the CRU TS dataset, whose reliability in Central Asia after 1930 has been confirmed in numerous studies (Duan et al., 2020). Consequently, our study period was defined as 1931–2024 to ensure simulation accuracy. To enhance the spatial precision of these climate inputs for smaller sub-basins, the CRU JRA data was downscaled to a finer 0.05° resolution. This was achieved using the delta-change statistical downscaling method with bias correctionBased on this confirmed post-1930 reliability, our study period was set from 1931 to 2024 to ensure the accuracy of our simulations. To enhance the precision of these climate inputs, particularly for smaller sub-basins, the CRU JRA data was downscaled to a finer 0.05° resolution. This was achieved using the delta-change statistical downscaling method with bias correction (Peng et al., 2019), leveraging the monthly TerraClimate dataset (1/24° resolution)—also derived from CRU TS—to ensure cross-dataset consistency. This downscaling procedure strictly enforces mass conservation, ensuring that the area-weighted sum of the fine-resolution precipitation matches the total water volume of the original coarse-resolution forcing.leveraging the monthly TerraClimate dataset (1/24° resolution), which is also derived from CRU TS, to ensure consistency across datasets.

To project future hydrological dynamics, we utilized climate projections from the NASA Earth Exchange Global Daily Downscaled Projections (NEX-GDDP-CMIP6) dataset. This dataset provides bias-corrected, high-resolution (0.25°) daily climate scenarios derived from the General Circulation Models (GCMs) of the Coupled Model Intercomparison Project Phase 6 (CMIP6). We selected an ensemble of six GCMs (ACCESS-CM2, BCC-CSM2-MR, CanESM5, EC-Earth3, MIROC6, and MPI-ESM1-2-HR) under three Shared Socioeconomic Pathways (SSPs): SSP1-2.6 (sustainability), SSP3-7.0 (regional rivalry), and SSP5-8.5 (fossil-fueled development). These specific models were selected based on their proven performance in reproducing historical climatology and capturing precipitation and temperature patterns in the arid regions of Central Asia, as

Formatted: Font: (Default) +Headings (Times New Roman)
Formatted: Font: (Default) +Headings (Times New Roman)
Formatted: Font: (Default) +Headings (Times New Roman)
Formatted: Font: (Default) +Headings (Times New Roman)
Formatted: Font: (Default) +Headings (Times New Roman)
Formatted: Font: (Default) +Headings (Times New Roman)
Formatted: Font: (Default) +Headings (Times New Roman)
Formatted: Font: (Default) +Headings (Times New Roman)

demonstrated in recent assessments (Alimkulov et al., 2025; Huang et al., 2024). The use of the multi-model ensemble mean (MME) further reduces the uncertainty associated with individual model structures.

This study also integrates multi-source observational data for both river discharge and lake dynamics. The observed streamflow dataset, provided by the National Cryosphere Desert Data Center and previous related studies,~~previous related studies (Duan et al., 2020; Guo et al., 2015)~~ includes monthly and yearly discharge records from 16 hydrological stations located on the main tributaries (locations shown in Fig. 1). These records vary in duration but collectively cover the 1931–2024 period, supporting the validation of our historical periodization (Appendix Table B1). For the lake, a long-term water level time series (1931–2024) was compiled to validate the water balance reconstruction. Historical gauge observations from 1931 to 2015 were obtained from ~~(~~Duan et al.~~,~~ (2020), while recent data (2016–2024) were extended using satellite altimetry products from the Global Reservoirs and Lakes Monitor (G-REALM). To derive the observed changes in lake water storage, we applied established water level-area-volume relationships, with the specific conversion curve displayed in Appendix Fig. A2 (Myrzakhmetov et al., 2022). These datasets allow for a robust closure of the water balance and validation of the simulated lake volume changes.

~~The observed streamflow dataset is provided by the National Cryosphere Desert Data Center and previous related studies (Duan et al., 2020; Guo et al., 2015).~~

2.3 Methodology

The core methodology of this study is the Hydrological Analysis and Disentanglement~~Attribution and Analysis~~ Framework (~~HAAF~~HADF), a structured three-stage process designed to clarify~~attribute~~ the causes of lake water volume changes. The workflow begins with hydrological process modeling in the catchment, followed by driver ~~attribution~~analysis, and concludes by linking these drivers to the lake's response. A conceptual flowchart of the HADF is presented in Fig. 3, and a detailed description of the three stages follows.~~Figure 2 shows a conceptual flowchart, and the following is a detailed description of the three stages.~~

Formatted: Font: (Default) +Headings (Times New Roman)

Formatted: Font: (Default) +Headings (Times New Roman)

Formatted: Font: (Default) +Headings (Times New Roman)

Formatted: Font: (Default) +Headings (Times New Roman)

Formatted: Font: (Default) +Headings (Times New Roman)

Formatted: Font: (Default) +Headings (Times New Roman)

Formatted: Font: (Default) +Headings (Times New Roman)

Formatted: Font: (Default) +Headings (Times New Roman), Font color: Auto

Formatted: Font: (Default) +Headings (Times New Roman), Font color: Auto

Formatted: Font: (Default) +Headings (Times New Roman)

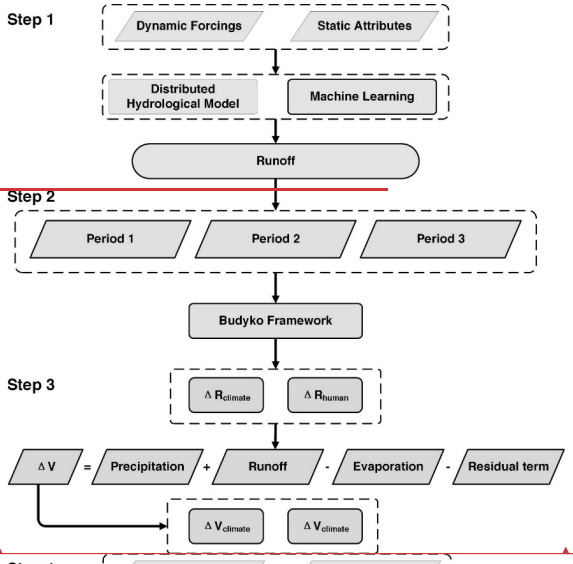

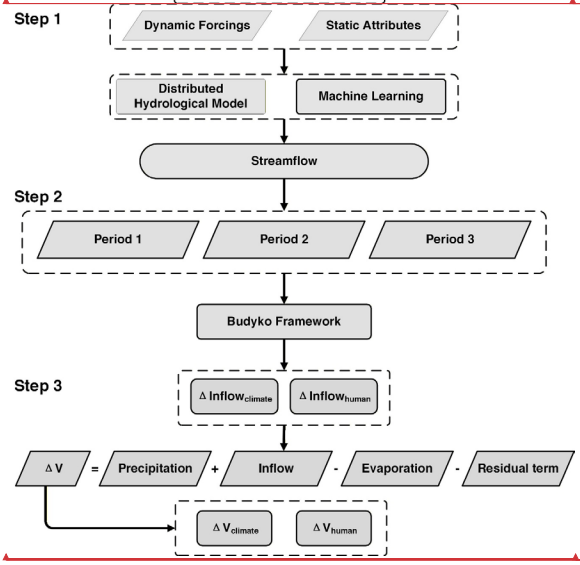

Formatted: Font: (Default) +Headings (Times New Roman)

Formatted: Font: (Default) +Headings (Times New Roman)

Formatted: Font: (Default) +Headings (Times New Roman)

Formatted: Font: (Default) +Headings (Times New Roman), (Asian) +Body Asian (宋体), 10 pt, (Asian) Chinese (Simplified, Mainland China)

Figure ~~1~~2~~:~~. Flowchart of the Hydrological Analysis and Disentanglement Framework (HADF). The framework consists of three steps: (1) Hybrid Hydrological Reconstruction, (2) Budyko-based Analysis, and (3) Lake System Response Linkage. Inputs include dynamic climate forcings and static attributes, while outputs quantify the relative contributions of climate ($\Delta V_{climate}$) and human activities (ΔV_{human}) to lake volume changes.

~~AAF Flowchart (Step 1: PIML-based Reconstruction, Step 2: Budyko Framework Attribution, Step 3: Lake System Response Linkage, with inputs like dynamic forcings and outputs like $\Delta V_{climate}$ and ΔV_{human}.)~~

2.3.1 Hybrid Hydrological Reconstruction Model

~~PIML-based Hydrological Reconstruction~~

To achieve reliable runoff reconstruction, this study employed a hybrid modeling framework that couples the process-based the sublimation-enhanced glacier SWAT+ (SEGSWAT+) model with a ML error-correction module. Unlike "black-box" approaches, this framework leverages the physical consistency of SEGSWAT+ (Yang et al., 2024) while utilizing the predictive capability of ML to minimize structural and forcing-induced errors. The SWAT model and its variants are extensively applied in hydrological simulations, including water resources management and pollution modelling (Forgrave et al., 2024; Ho et al., 2025; Sánchez-Gómez et al., 2025). Notably, in simulations involving complex cryospheric processes (snow and ice), coupling physical models with external correction modules typically yields significant performance improvements. Hybrid modeling based on this approach is increasingly recognized for its robustness in data-scarce regions and has demonstrated superior performance in the Lake Balkhash basin compared to standalone models. The workflow proceeds in two distinct stages, as illustrated in (Fig. 4). First, the SEGSWAT+ model was independently calibrated using observed streamflow. This model utilizes static attributes and dynamic forcings to simulate the baseline hydrological processes, including glacial melt and evapotranspiration. Subsequently, the residuals (Q_{res})—defined as the discrepancy between the SEGSWAT+ simulated streamflow (Q_{sim}) and observed streamflow (Q_{obs})—were calculated. A suite of ML algorithms was then trained to predict these residuals (Q_{res_sim}) based on a set of predictors, including meteorological inputs and SEGSWAT+ state variables. The final reconstructed runoff is the sum of the physical model output and the ML-predicted residual. This strategy effectively functions as a non-linear bias correction. Overfitting, a common concern in ML, is mitigated here because the ML component targets only the residuals rather than the total flow. Since the residuals from a calibrated physical model are inherently bounded and smaller in magnitude than the total runoff, the search space for the ML model is constrained, preserving the physical plausibility of the final output.

For the ML component, we employed a diverse ensemble of architectures: Artificial Neural Networks (ANN), Long Short-Term Memory (LSTM), Random Forest (RF), and XGBoost (Behrouz et al., 2022; Guo et al., 2023; Srinivasulu and Jain, 2006; Wang and Peng, 2024). Hyperparameters for each model were optimized using a grid search strategy (details in Appendix Table B2). The dataset for each period was split into training (70%) and validation (30%) subsets. To evaluate performance, we utilized four metrics: the Kling-Gupta Efficiency (KGE), Nash-Sutcliffe Efficiency (NSE), Percent Bias (PBIAS), and Coefficient of Determination (R^2). In cases where metrics yielded conflicting assessments, the KGE was prioritized as the primary selection criterion due to its balanced decomposition of correlation, bias, and variability errors, with

Formatted: Font: (Default) +Headings (Times New Roman), 10 pt
Formatted: Font: 10 pt
Formatted: Font: 10 pt
Formatted: Font: 10 pt
Formatted: Font: (Default) +Headings (Times New Roman), 10 pt
Formatted: Font: 10 pt
Formatted: Font: 10 pt
Formatted: Font: 10 pt
Formatted: Font: (Default) +Headings (Times New Roman), 10 pt
Formatted: Font: (Default) +Headings (Times New Roman)
Formatted: Font: (Default) +Headings (Times New Roman)
Formatted: Font: (Default) +Headings (Times New Roman)
Formatted: Font: (Default) +Headings (Times New Roman)
Formatted: Font: (Default) +Headings (Times New Roman)
Formatted: Font: (Default) +Headings (Times New Roman)
Formatted: Font: (Default) +Headings (Times New Roman)
Formatted: Font: (Default) +Headings (Times New Roman)
Formatted: Font: (Default) +Headings (Times New Roman)
Formatted: Font: (Default) +Headings (Times New Roman)
Formatted: Font: (Default) +Headings (Times New Roman), Superscript
Formatted: Font: (Default) +Headings (Times New Roman)

PBIAS acting as a constraint to ensure water balance closure. The best-performing ML model was selected to generate the final historical streamflow series. To quantitatively demonstrate the improvement achieved by this hybrid approach, a detailed comparison of performance metrics between the raw SEGSWAT+ output and the final hybrid model across training and validation phases is provided in Appendix Table B3.

~~Physics-informed machine learning (PIML) integrates conceptual hydrological models with machine learning (ML) to synergistically leverage the predictive power of ML algorithms and the process-based understanding of physical models (Bhasme et al., 2022). This integration also enhances the model's physical consistency and interpretability. The SWAT model and its improved versions are widely used in hydrological simulation processes. In our framework, we employed the Sublimation-Enhanced Glacier SWAT+ model (SEGSWAT+), which is an iteration of the SWAT model specifically adapted for glacial hydrology and has been proven effective for simulating the glacially-influenced runoff in the Lake Balkhash basin (Yang et al., 2024). By combining inputs (precipitation, potential evapotranspiration), state variables (groundwater storage, soil moisture), and intermediate outputs (actual evapotranspiration) leading to a target variable (simulated runoff at specific gauge locations). Subsequently, a suite of ML methods competed to learn the residuals—the discrepancies between SEGSWAT+ simulated runoff and observed streamflow—to correct and improve the final output accuracy. The architecture of our PIML framework is illustrated in Fig. 3. The rationale for this PIML design is that the residual between a model prediction and an observation represents a composite error stemming from inherent limitations of the process-based hydrological model and uncertainties in driving data. By learning these complex residual patterns, the ML component enhances hydrological accuracy without severe overfitting biases, as residuals from a reliable physical model are inherently bounded and cannot exceed the runoff magnitude, constraining the ML model and preserving physical plausibility.~~

~~For the ML component, we employed a diverse ensemble of architectures common in hydrology and Earth science applications, including Artificial Neural Networks (ANN), Long Short-Term Memory (LSTM) networks, Random Forest (RF), and XGBoost (Behrouz et al., 2022; Guo et al., 2023; Srinivasulu and Jain, 2006; Wang and Peng, 2024). The best-performing model from this competitive ensemble was selected for each simulation period, a method known for its robustness in capturing water balance dynamics. The proposed PIML model was run for the three distinct periods, calibrated using multi-objective functions (including Kling-Gupta Efficiency (KGE), Nash-Sutcliffe Efficiency (NSE), and percent bias) against data from 16 hydrological stations, with cross-validation to ensure generalizability.~~

Formatted: Indent: First line: 2 ch, Don't adjust right indent when grid is defined, Don't snap to grid

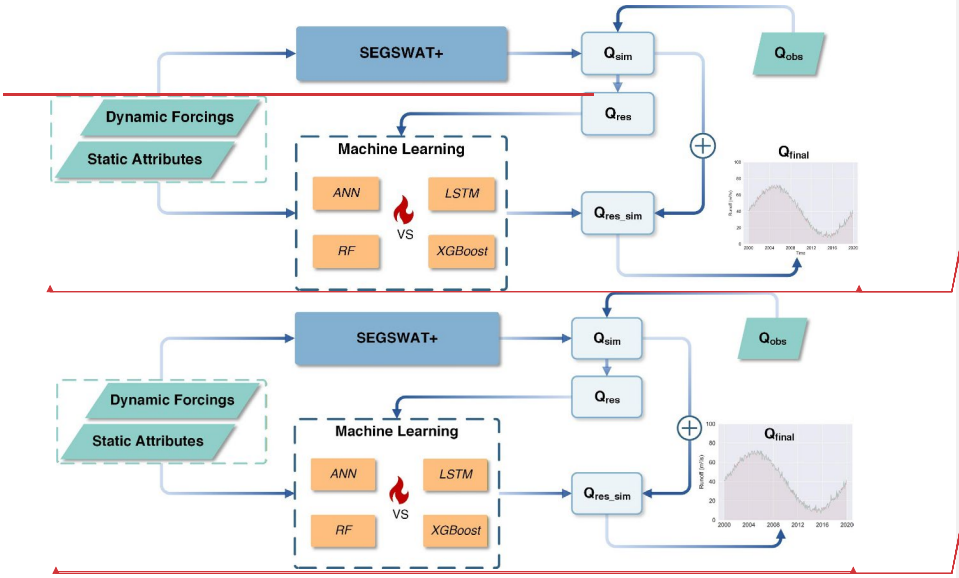

Figure ~~3~~ 4. ~~PIML structure~~Hybrid hydrological modeling structure

2.3.2 Budyko-based ~~Driver Attribution~~Contribution Analysis

To quantitatively distinguish the impacts of climate change from those of direct human activities on streamflow~~runoff~~, we employed the Budyko framework (Budyko and Miller, 1974). This framework provides a robust, first-order approximation of the long-term water balance in a catchment by describing the partitioning of precipitation (P) into actual evapotranspiration (ET) and streamflow~~runoff~~ (Q). Its core hypothesis is that the ratio of actual evapotranspiration to precipitation (ET/P) is primarily a function of the aridity index (Φ), defined as the ratio of potential evapotranspiration (ET_0) to precipitation (P). The total change in mean annual streamflow~~runoff~~ (ΔQ) between a baseline and an altered period can be decomposed into contributions from climate change (ΔQ_c) and direct human activities (ΔQ_h). For this decomposition, we adopted a climate elasticity method (Dooge et al., 1999). This method approximates the contribution of any controlling factor x (such as rainfall, snowmelt, etc.) ~~x (e.g., the precipitation P)~~ to ~~the total runoff change (~~ΔQ~~)~~ as the product of the change in that factor (Δx) and the sensitivity of streamflow~~runoff~~ to that factor ($\partial Q/\partial x$). This relationship is mathematically grounded in the widely used Choudhury-Yang equation~~This relationship is mathematically grounded in the widely used Choudhury-Yang equation~~ (Yang et al., 2008), expressed as:~~i.e., Equation 1, which is a one-parameter form of the Budyko curve:~~

Formatted: Font: (Default) +Headings (Times New Roman)
Formatted: Font: (Default) +Headings (Times New Roman), 10 pt
Formatted: Font: (Default) +Headings (Times New Roman)
Formatted: Font: (Default) +Headings (Times New Roman), 10 pt
Formatted: Font: (Default) +Headings (Times New Roman)
Formatted: Font: (Default) +Headings (Times New Roman)
Formatted: Font: (Default) +Headings (Times New Roman)
Formatted: Font: (Default) +Headings (Times New Roman)
Formatted: Font: (Default) +Headings (Times New Roman)
Formatted: Font: (Default) +Headings (Times New Roman)
Formatted: Font: (Default) +Headings (Times New Roman)
Formatted: Font: (Default) +Headings (Times New Roman)
Formatted: Font: (Default) +Headings (Times New Roman)
Formatted: Font: (Default) +Headings (Times New Roman)
Formatted: Font: (Default) +Headings (Times New Roman)
Formatted: Font: (Default) +Headings (Times New Roman)
Formatted: Font: (Default) +Headings (Times New Roman)

$$\frac{ET}{P} = \frac{1}{[1+(P/ET_0)^n]^{1/n}} \quad (1)$$

This equation features a single catchment parameter, n, which represents the integrated control of the underlying landscape characteristics (e.g., vegetation, soil, topography) on the partitioning of effective precipitation into ~~runoff~~ streamflow and evapotranspiration. In this study, the parameter n was calibrated for each period by solving Equation (1) inversely, using the period-averaged P, ET_0, and observed ET (derived from the water balance equation ET=P−Q over the long term). ET_0 was calculated using the Penman-Monteith method (Jackson et al., 1981) based on the meteorological variables sourced from the climate driver dataset described in Section 2.2. Consequently, the change in this parameter (Δn) between periods can be interpreted as the integrated effect of direct human activities that alter these landscape properties (e.g., land use change, reservoir construction).

Following this framework, ~~the total runoff change (ΔQ)~~ can be partitioned into contributions from changes in climatic variables (rainfall, snowmelt, glacial melt, ET_0) and human-induced landscape changes (represented by Δn). The sensitivity coefficients of streamflow~~runoff~~ to each of these factors are detailed in Equations (2a-2c), and equation (3) provides a comprehensive expression:

$$\frac{\partial ET}{\partial P} = \frac{ET}{P}\left(\frac{ET_0^n}{ET_0^n+P^n}\right) \quad (2a)$$

$$\frac{\partial ET}{\partial ET_0} = \frac{ET}{ET_0}\left(\frac{P^n}{ET_0^n+P^n}\right) \quad (2b)$$

$$\frac{\partial ET}{\partial n} = \frac{ET}{n}\left(\frac{\ln(ET_0^n+P^n)}{n} - \frac{ET_0^n \ln ET_0 + P^n \ln P}{ET_0^n+P^n}\right) \quad (2c)$$

$$\Delta Q = \left(1 - \frac{\partial ET}{\partial P}\right)\Delta P - \frac{\partial ET}{\partial ET_0}\Delta ET_0 - \frac{\partial ET}{\partial n}\Delta n \quad (3)$$

2.3.3 Lake System Response Linkage

The final stage of the HADF explicitly links catchment-scale drivers to the observed changes in the lake's water storage. The change in Lake Balkhash's water storage (ΔV) over a defined period (Δt) is essentially determined by the balance between water inflow and water dissipation. Its water balance equation can be expressed as follows:

$$\frac{\Delta V}{\Delta t} = A(h)(P - ET) + Q_{in} \quad (4)$$

Where A is the lake surface area, which is a function of water level (h), Q_{in} is the inflow. ~~The time series of annual water levels for Lake Balkhash during the study period was obtained from the work of Nakayama et al. (1997) and Duan et al. (2020). Subsequently, the corresponding lake surface area time series was derived using the level-to-area conversion function provided by the former.~~ The ΔV was then calculated based on the methodology established by Zhang et al. (2013), an approach whose

Formatted: Font: (Default) +Headings (Times New Roman)
Formatted: Don't adjust right indent when grid is defined, Don't snap to grid
Formatted: Font: (Default) +Headings (Times New Roman), Subscript
Formatted: Font: (Default) +Headings (Times New Roman)
Formatted: Font: (Default) +Headings (Times New Roman), Subscript
Formatted: Font: (Default) +Headings (Times New Roman)
Formatted: Font: (Default) +Headings (Times New Roman)
Formatted: Font: (Default) +Headings (Times New Roman)
Formatted: Font: (Default) +Headings (Times New Roman)
Formatted: Font: (Default) +Headings (Times New Roman)
Formatted: Font: (Default) +Headings (Times New Roman)
Formatted: Font: (Default) +Headings (Times New Roman)
Formatted: Font: (Default) +Headings (Times New Roman)
Formatted: Font: (Default) +Headings (Times New Roman)
Formatted: Font: (Default) +Headings (Times New Roman)
Formatted: Font: (Default) +Headings (Times New Roman)
Formatted: Font: (Default) +Headings (Times New Roman)
Formatted: Font: (Default) +Headings (Times New Roman)

reliability for Lake Balkhash has been previously validated (Wang et al., 2022). The latter calculated the water volume change using the following formula, referencing interannual variations in lake surface elevation and area:

$$\Delta V = \frac{1}{3(H_1 - H_2)} \times \left(A_1 + A_2 + \sqrt{A_1 \times A_2}\right) \quad (5)$$

In the equation: ΔV represents the change in lake volume from surface elevation H_1 and area A_1 to elevation H_2 and area A_2. ~~It is important to note that, given the long-term temporal scale of this study, the exchange between the lake and surrounding groundwater systems was considered negligible and thus omitted from the water balance calculations.~~ Previous hydrogeological assessments of Lake Balkhash suggest that net groundwater exchange constitutes a minor fraction of the total water budget compared to the dominant surface inflow and evaporative fluxes (Deng et al., 2011~~, p.60~~; Wang et al., 2022). Therefore, the lake-groundwater exchange was assumed negligible in this study. This simplification allows for a focused attribution of the primary surface drivers.

The final stage of the ~~HAAF~~ HADF connects the ~~attribution~~ results from Stage 2 to the observed changes in the lake's water storage, thereby achieving an end-to-end assessment ~~attribution~~. This linkage is achieved through the lake's water balance equation. The total change in lake storage (ΔV_{obs}) between two periods (e.g., an altered period vs. a baseline period) can therefore be expressed as:

$$\Delta V_{obs} = \Delta Q_{in} + \Delta P - \Delta ET$$

(~~5~~6)

The key innovation in Stage 3 is to decompose this total storage change into contributions from climate change and human activities. We achieve this by substituting the ~~attributed~~ inflow~~runoff~~ changes from Stage 2 into Equation ~~(5~~6). The ΔQ_{in} was already separated into ΔQ_c and ΔQ_h components. Changes in lake precipitation and lake evaporation are, by definition, driven by climatic factors. Therefore, we can re-organize the ~~c~~Equation ~~(5)~~ to separate ~~the total storage change (ΔV_{obs})~~ into its climatic (ΔV_c) and human-activity (ΔV_h) driven components:

$$\Delta V_c = \Delta Q_c + \Delta P - \Delta ET \quad (~~6a~~7a)$$

$$\Delta V_h = \Delta Q_{in} ~~+ \Delta P - \Delta E~~ \quad (~~6b~~7b)$$

Equations (7a) and (7b) represent the core of the "impact propagation" within the HADF. This formulation allows for a quantitative determination of how much of the observed change in the lake's total water volume is attributable to natural climate variability (acting on both the catchment and the lake surface) versus direct human activities. This provides a system-level quantitative explanation for the lake's historical dynamics.

~~This set of equations (6a and 6b) represents the core of the "attribution transference" in the HAAF framework. It allows us to quantitatively determine how much of the observed change in the lake's total water volume is due to natural climate variability (acting on both the catchment and the lake itself) and how much is due to direct human activities. This provides a complete, system-level quantitative explanation for the lake's historical dynamics.~~

Formatted: Font: (Default) +Headings (Times New Roman)
Formatted: Font: (Default) +Headings (Times New Roman)
Formatted: Font: (Default) +Headings (Times New Roman)
Formatted: Font: (Default) +Headings (Times New Roman)
Formatted: Font: (Default) +Headings (Times New Roman)
Formatted: Font: (Default) +Headings (Times New Roman)
Formatted: Font: (Default) +Headings (Times New Roman)
Formatted: Font: (Default) +Headings (Times New Roman)
Formatted: Don't adjust right indent when grid is defined, Don't snap to grid
Formatted: Font: (Default) +Headings (Times New Roman)
Formatted: Font: (Default) +Headings (Times New Roman)
Formatted: Font: (Default) +Headings (Times New Roman)
Formatted: Font: (Default) +Headings (Times New Roman)
Formatted: Font: (Default) +Headings (Times New Roman)
Formatted: Font: (Default) +Headings (Times New Roman)
Formatted: Font: (Default) +Headings (Times New Roman)
Formatted: Font: (Default) +Headings (Times New Roman)
Formatted: Font color: Auto, Portuguese (Brazil)
Formatted: Font color: Auto, Portuguese (Brazil)
Formatted: Font: (Default) +Headings (Times New Roman)

~~2.3.4 Model Evaluation and Uncertainty Metrics~~

~~The hydrological simulation performance of the PIML model was rigorously evaluated by comparing the simulated daily and monthly streamflow against observed data. For this purpose, we selected three widely used metrics: the Coefficient of Determination (R2), the Kling-Gupta Efficiency (KGE), Percent Bias (PBIAS), and the Nash-Sutcliffe Efficiency of the logarithm of streamflow (logNSE) (Yang et al., 2023). To evaluate the agreement between simulated and observed values, the R2 was calculated, which measures the proportion of the variance in the dependent variable that is predictable from the independent variables. KGE is a comprehensive metric that decomposes model performance into three distinct components: correlation (r), bias ratio (β), and variability ratio (γ). This decomposition allows for a more nuanced diagnosis of model deficiencies by distinguishing between errors in timing (correlation), overall water balance (bias), and flow dynamics (variability). KGE is calculated as follows:~~

$$KGE = 1 - \sqrt{(r-1)^2 + (\beta-1)^2 + (\gamma-1)^2} \quad (7)$$

~~where $\beta = \mu_s/\mu_o$ and $\gamma = (\frac{\sigma_s}{\mu_s})/(\frac{\sigma_o}{\mu_o})$. μ and σ represent the mean and standard deviation of the simulated (s) and observed (o) streamflow, respectively, and r is the Pearson correlation coefficient between them. A KGE value greater than -0.41 is generally considered acceptable for hydrological modeling, indicating that the model performs better than the mean flow benchmark. PBIAS measures the average tendency of the simulated data to be larger or smaller than their observed counterparts, providing a straightforward assessment of model bias. It is calculated as:~~

$$PBIAS = \sum_{i=1}^{n} \frac{Q_{sim} - Q_{obs}}{Q_{obs}} \times 100 \quad (8)$$

~~where Q_{sim} represents the simulated runoff and Q_{obs} represents the observed runoff. A PBIAS value within the range of $\pm$25% is typically considered satisfactory, with values closer to 0 indicating better model performance. The $log\ NSE$ is a modification of the standard Nash-Sutcliffe Efficiency (NSE) that is particularly sensitive to model performance during low-flow periods. This is critically important for hydrological modeling in arid and semi-arid regions. It is calculated as:~~

$$log\ NSE = 1 - \frac{\sum_{i=1}^{n}(log\ Q_{sim} - log\ Q_{obs})^2}{\sum_{i=1}^{n}(log\ Q_{obs} - \overline{log\ Q_{obs}})^2} \quad (9)$$

~~where $\overline{\log Q_{obs}}$ represents the mean of the logarithm of the runoff observations. A $log\ NSE$ value greater than 0.36 is generally considered to indicate a satisfactory to good model performance for low-flow simulations.~~

3. Results

3.1 Hydrological Model Performance Evaluation

~~Accurate hydrological runoff modeling is the first step in HAAF. Based on the PIML model, parameterization is performed by combining field measurements, geospatial datasets, and remote sensing products (e.g., topographic data, soil texture maps,~~

Formatted: Normal

Formatted: Font: (Default) +Headings (Times New Roman), Font color: Auto

Formatted: Font: (Default) +Headings (Times New Roman)

~~and soil hydraulic parameters). The calibrated parameters included: (1) snow module parameters (critical melt temperature and degree-day factors); (2) vegetation and land surface parameters (root depth, soil anisotropy ratio, surface depression storage capacity, and surface roughness); and (3) glacier module parameters (critical melt temperature, degree-day factors, and area-volume scaling parameters. Detailed calibration parameters can be referenced in the study by Yang et al (2022). Model calibration and validation were performed independently for each of the three study periods, resulting in three distinct parameter sets. Notably, the parameter set for P1 was specifically configured to simulate naturalized streamflow under conditions free of significant human intervention. For each period and station, the available observed streamflow data were partitioned into calibration (70%) and validation (30%) subsets.~~

~~The predictive performance of machine learning models was evaluated using the R2 metric to determine the optimal model for modeling the residual runoff (Fig. 4). While the Random Forest (RF), Long Short-Term Memory (LSTM), and XGBoost models all demonstrated high predictive accuracy, with respective R2 values of 0.865, 0.863, and 0.912, XGBoost distinguished itself. Its predictions not only achieved the highest coefficient of determination but were also the most tightly clustered around the 1:1 reference line, indicating superior stability and minimal variance. In contrast, the Artificial Neural Network (ANN) exhibited inferior performance (R2 = 0.810), characterized by a widely scattered data distribution and significant deviation from the 1:1 line, which suggests substantial bias. Given its superior accuracy and reliability, XGBoost was therefore selected as the optimal model to adjust the final streamflow simulations.~~

Accurate hydrological modeling forms the foundation of the HADF. Parameterization of the process-based SEGSWAT+ module was conducted by integrating the topographic, soil, and land use datasets described in Section 2.2. The key calibrated parameters included: (1) snow module parameters (e.g., critical melt temperature, degree-day factors); (2) vegetation and land surface parameters (e.g., root depth, soil anisotropy ratio, surface roughness); and (3) glacier module parameters (e.g., area-volume scaling coefficients). A detailed description of the calibration protocol and parameter ranges follows the methodology established by Yang et al (2022). Model calibration and validation were performed independently for each of the three historical periods, yielding distinct parameter sets. Notably, the parameter set for the Reference Period (P1) was specifically configured to capture naturalized runoff conditions, minimizing the influence of intensive human intervention.

The predictive performance of the candidate machine learning models was evaluated using the R^2 to identify the optimal architecture for residual correction (Fig. 5). While RF, LSTM, and XGBoost all demonstrated high accuracy, with R^2 values of 0.865, 0.863, and 0.912, respectively, XGBoost outperformed the others. As shown in the scatter plots, XGBoost predictions were most tightly clustered around the 1:1 reference line, indicating superior stability and minimal variance. In contrast, the ANN exhibited lower performance (R^2 = 0.810), characterized by greater scatter and deviation, suggesting substantial bias. Consequently, XGBoost was selected as the optimal regressor for the residual correction module in the final hybrid model.

Formatted: Font: (Default) +Headings (Times New Roman)

Formatted: Font: (Default) +Headings (Times New Roman)

Formatted: Font: (Default) +Headings (Times New Roman), Superscript

Formatted: Font: (Default) +Headings (Times New Roman)

Formatted: Font: (Default) +Headings (Times New Roman)

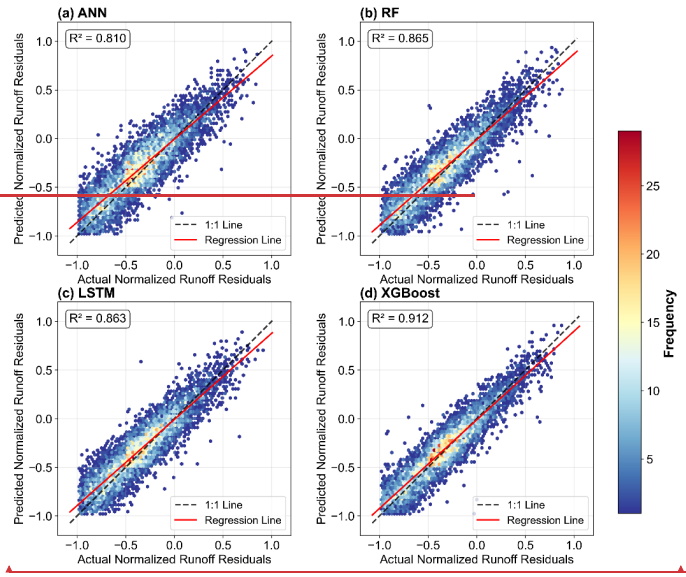

Formatted: Font: (Default) +Headings (Times New Roman)

Formatted: Font: (Default) +Headings (Times New Roman), 10 pt

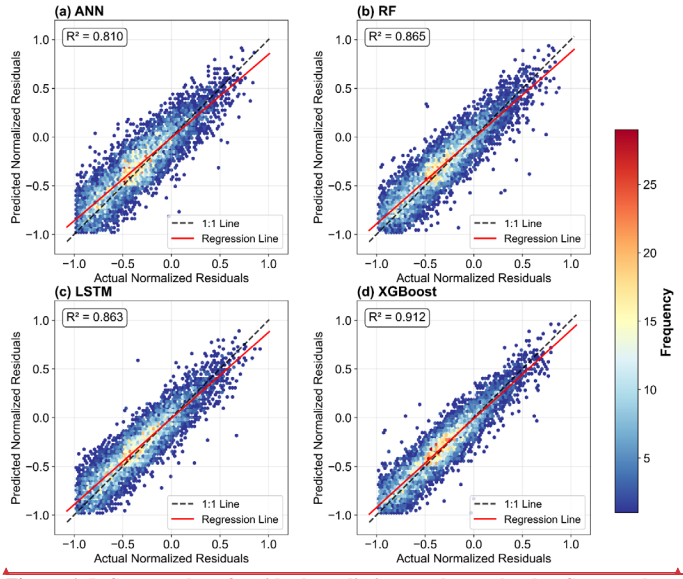

Figure ~~4~~ 5. ~~Scatter plot of residual predictions and actual values~~Scatter plots comparing machine learning model predictions of runoff residuals against actual residuals. The solid black line represents the 1:1 reference line.

~~Based on the optimal machine learning model, the final runoff results obtained were compared with the measured runoff data through a multi-indicator assessment. The comprehensive performance assessment results are shown in Fig. 5. The first ten hydrological stations, which control the main stem of the Ili River, demonstrated strong model performance. For all these stations, KGE values exceeded 0.75, PBIAS was within ±10%, and logNSE was above 0.7, indicating an excellent fit to the observed runoff. Specifically, the Ushzharma station, located at the river's terminus just before it enters the lake, exhibited outstanding performance with a KGE of 0.847, a low bias (PBIAS = 5.1%), and exceptional skill in simulating low flows (logNSE = 0.929). The remaining stations, which monitor the four eastern tributary rivers, showed similarly robust results. KGE values were consistently above 0.8 and PBIAS remained within ±10%. Except for the Chiganak station, where the logNSE of 0.699 is still considered indicative of good low-flow simulation, all other eastern stations achieved logNSE values greater than 0.7. This confirms that the model accurately simulates runoff for all major rivers flowing into the eastern part of the lake. This robust performance establishes a solid foundation for the subsequent lake water balance calculations and the application of the Budyko framework for attribution analysis.~~

The final reconstructed runoff, generated by the optimized hybrid model, was validated against observed data using a multi-metric assessment (Fig. 6). The model demonstrated robust performance across the basin. For the ten stations along the main

Formatted: Font: (Default) +Headings (Times New Roman)

Formatted: Font: (Default) +Headings (Times New Roman), 10 pt

Formatted: Font: (Asian) +Body Asian (宋体), (Asian) Chinese (Simplified, Mainland China)

Formatted: Normal

Formatted: Font: (Default) +Headings (Times New Roman)

Formatted: Indent: First line: 0 ch

stem of the Ili River, KGE values consistently exceeded 0.75, PBIAS remained within ±10%, and logNSE values were above 0.7, indicating an excellent fit to observed hydrographs. Specifically, at the Ushzharma station—the critical control point at the river's terminus—the model achieved outstanding performance with a KGE of 0.847, minimal bias (PBIAS = 5.1%), and exceptional skill in capturing low-flow dynamics (logNSE = 0.929). Similarly, the four stations monitoring the eastern tributaries (Karatal, Aksu, Lepsy, and Ayaguz rivers) exhibited strong agreement with observations, with KGE values consistently exceeding 0.8 and PBIAS within ±10%. Even at the Chiganak station, a logNSE of 0.699 indicates reliable low-flow simulation, while all other eastern stations surpassed 0.7. These results confirm that the hybrid model accurately reproduces hydrological processes across spatially heterogeneous sub-basins, establishing a solid foundation for the subsequent lake water balance reconstruction and driver separation analysis.

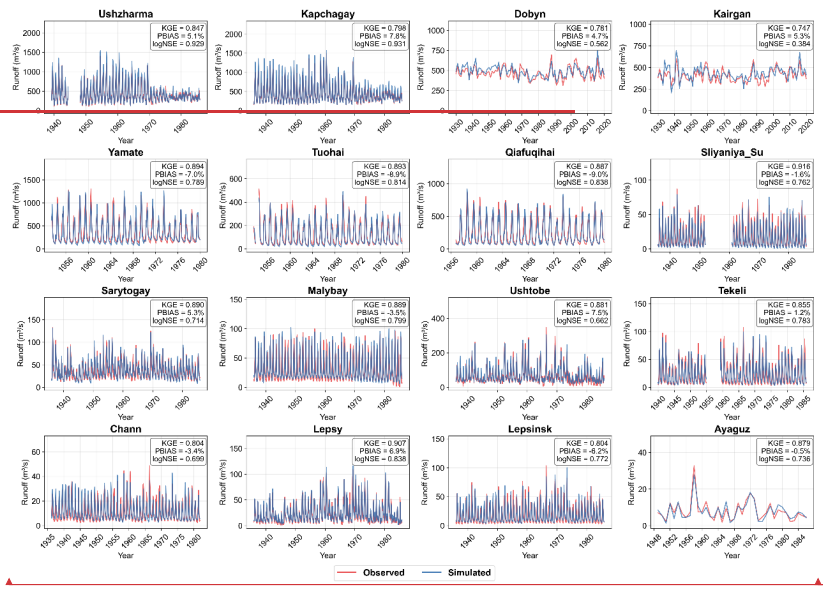

Formatted: Font: (Default) +Headings (Times New Roman), (Asian) +Body Asian (宋体), English (United States)

Formatted: Font: (Default) +Headings (Times New Roman), English (United Kingdom)

Formatted: Font: (Default) +Headings (Times New Roman)

Formatted: Font: (Default) +Headings (Times New Roman), 10 pt

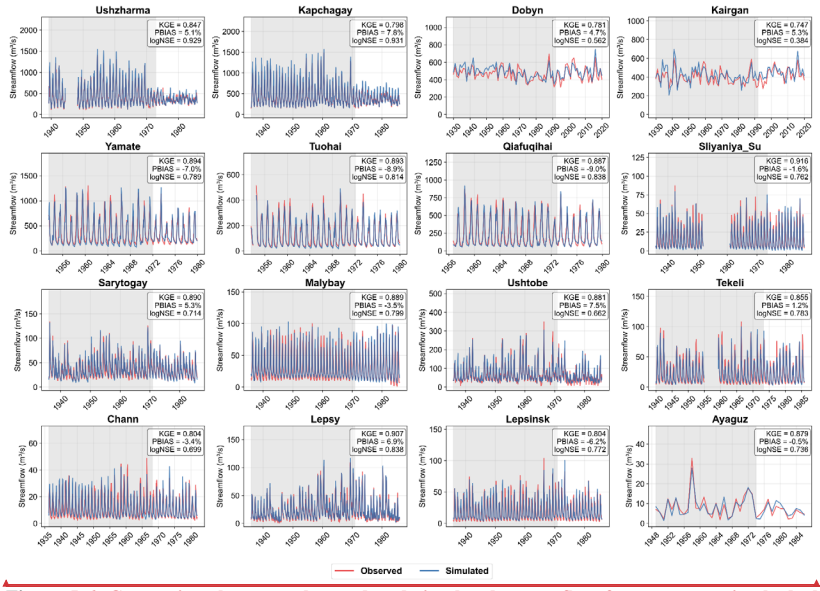

Figure ~~5~~ 6. Comparison between observed and simulated streamflow for representative hydrological stations. The shaded gray background indicates the calibration period, while the unshaded area represents the validation period.~~Results of the runoff fitting assessment~~

3.2 Quantification of The Impacts on Variations in Streamflow~~Runoff~~

~~The total runoff into Lake Balkhash was calculated as the sum of simulated streamflow from all modeled tributary rivers, adjusted for deltaic water consumption using the methodology of Thevs et al. (2016). The simulation strategy to generate the final time series was as follows:~~ The total inflow into Lake Balkhash was calculated as the sum of simulated streamflow from all modeled tributary rivers, adjusted for transmission losses in the delta. Deltaic water consumption was estimated using the empirical function derived by ~~(~~Xie et al.~~,~~ ~~(~~2011), which correlates water losses with inflow volume based on historical observations (detailed equation provided in Appendix equation C1). To reconstruct the continuous inflow time series, we implemented a two-scenario simulation strategy. First, Naturalized Inflow~~Runoff~~ (Q_{nat}~~$Qnat$~~~~,~~ was simulated to isolate the catchment's hydrological response to climate variability under "pre-disturbance" landscape conditions. This was achieved by applying the model parameter set calibrated for the Reference Period (P1, 1931-1969)—representing a state of minimal human interference—to the entire study period (1931-2024), driven by actual dynamic meteorological forcings. While this standard "fixed-parameter" approach effectively isolates climatic signals, we acknowledge that it assumes stationary physical properties

Formatted: Font: (Default) +Headings (Times New Roman)

Formatted: Font: (Default) +Headings (Times New Roman), 10 pt

Formatted: Font: (Default) +Headings (Times New Roman), (Asian) +Body Asian (宋体), (Asian) Chinese (Simplified, Mainland China)

Formatted: Normal

Formatted: Font: (Default) +Headings (Times New Roman)

Formatted: Font: (Default) +Headings (Times New Roman)

(e.g., glacier parameters) over time; the implications of this assumption regarding cryospheric dynamics are critically examined in the Discussion section. Second, ~~the parameter set calibrated for the baseline period (P1) was used to simulate naturalized streamflow across the entire study period (1931-2024).~~ Actual Inflow ~~Human-Impacted Runoff~~ (Q_{act} ~~Qreal~~), was reconstructed to represent the historical reality of water entering the lake. For the periods of intensive human activity (P2 and P3), the model was updated with distinct parameter sets calibrated specifically for 1970-1990 and 1991-2024, respectively, to capture the evolving anthropogenic footprint. To ensure maximum accuracy, this reconstructed series prioritizes observations: direct gauge records were used whenever available, with simulated values employed solely to fill gaps in the observational record. The resulting reconstructed time series for both natural and actual inflow are presented in Fig. 7.~~the construction of the historical, human-impacted runoff series involved a multi-step process. The parameter set for P2 was used to simulate runoff for both the P1 and P2 periods (1931-1990), while the P3 parameter set was applied exclusively to its own period (1991-2024). For any year where direct observational data were available, these records superseded the simulated values to create the final composite Qreal series. The results of the reconstruction of interannual natural runoff and actual runoff over nearly a century are shown in Fig. 6.~~

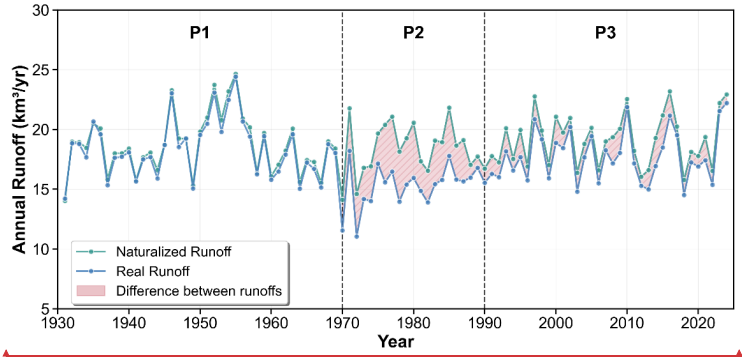

Formatted: Font: (Default) +Headings (Times New Roman)

Formatted: Font: (Default) +Headings (Times New Roman), 10 pt

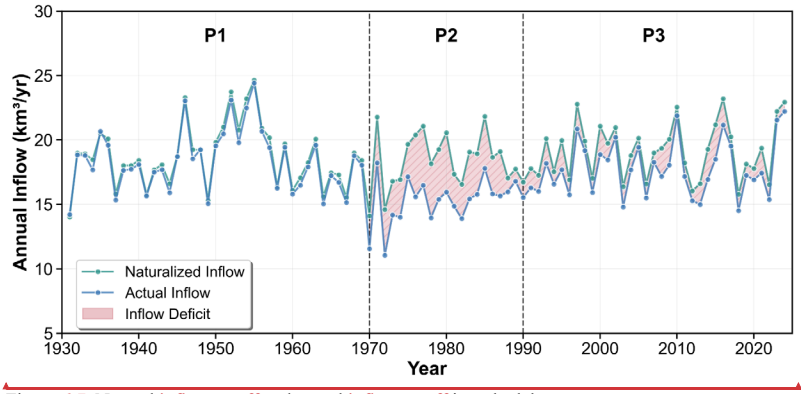

Figure ~~6~~ 7. Natural inflow~~runoff~~ and actual inflow~~runoff~~ into the lake

During the baseline period (1931-1969), the Q_{nat} ~~$Qnat$~~ and Q_{act} ~~Qreal~~ time series exhibited a close correspondence, tracking inter-annual fluctuations with high fidelity. Analysis of the deviations between naturalized and actual streamflow reveals a distinct three-stage evolution of human impact. During P1, the streamflow deficit was minimal, with a mean deviation of only 0.36 km³/yr. The narrow range between the maximum (0.99 km³/yr) and minimum (-0.19 km³/yr) differences indicates that observed flow closely aligned with natural conditions.~~time series exhibit a remarkably close correspondence, tracking each other's inter-annual fluctuations with high fidelity. Analysis of the deviations between naturalized (Qnat) and observed (Qreal) runoff reveals a distinct three-stage evolution of human impact on the basin's hydrology. During the baseline period (P1, 1931-1969), the runoff deficit was minimal, with a mean deviation of only 0.48 km³/yr. The small range between the maximum (1.29 km³/yr) and minimum (-0.19 km³/yr) differences indicates that the observed flow was closely aligned with natural conditions, fluctuating slightly around the naturalized values. In stark contrast, the intensive intervention period (P2, 1970-1990) marked a dramatic and persistent shift. The mean runoff deficit surged to 3.11 km³/yr, and critically, the minimum deviation remained positive (0.93 km³/yr), signifying a systematic and sustained reduction in flow throughout every year of this period, directly attributable to the onset of large-scale human activities. Following this, the compounded stress period (P3, 1991-2024) exhibited a more complex pattern. The mean runoff deficit decreased to 1.35 km³/yr, substantially lower than in P2, suggesting a partial mitigation or a shift in human impact, possibly due to changes in water management policies. Overall, the statistical progression clearly quantifies the transition from a near-natural state to a period of intense, sustained water withdrawal, and finally to a recent era characterized by reduced average impact but greater variability and more extreme events.~~ In contrast, the intensive intervention period (P2, 1970-1990) marked a substantial shift. The mean streamflow deficit increased to 3.11 km³/yr, and notably, the minimum deviation remained positive (0.93 km³/yr), signifying a systematic reduction in flow throughout this period, consistent with the onset of large-scale water withdrawals. Subsequently, the compounded pressures

Formatted: Font: (Default) +Headings (Times New Roman)

Formatted: Font: (Default) +Headings (Times New Roman), 10 pt

Formatted: Font: (Default) +Headings (Times New Roman)

Formatted: Font: (Default) +Headings (Times New Roman)

Formatted: Indent: First line: 0 ch

period (P3, 1991-2024) exhibited a more complex pattern. The mean streamflow deficit decreased to 1.35 km³/yr, suggesting a partial mitigation or shift in human impact, possibly linked to changes in water management policies. Overall, the statistical progression quantifies the transition from a near-natural state to a period of sustained high water withdrawal, and finally to a recent era characterized by reduced average impact but increased inter-annual variability.

The Budyko framework was employed to diagnose the hydro-climatic shifts between the three periods and to quantitatively separate the drivers of streamflow changes. The basin's evolutionary trajectory in the Budyko space is shown in Fig. 8(a). Based on a calibrated catchment parameter (n) of 1.776, the analysis confirms the dominant role of human activities in altering the basin's hydrology, particularly during the intensive intervention period. From the baseline period (P1) to the period of intensive alteration (P2), total observed streamflow decreased by 0.31 km³/yr. Our results indicate that direct human activities were the primary driver of this decline, accounting for -0.27 km³/yr, or 86.3% of the total change. Notably, this occurred while the climate became slightly less arid (aridity index ϕ decreased from 1.404 to 1.349). This finding underscores that the hydrological deficit during this era was not a consequence of adverse climate conditions but was largely driven by anthropogenic water withdrawals, consistent with the operation of the Kapchagay Reservoir.

~~The Budyko framework was employed to diagnose the hydro-climatic shifts between the three periods and to quantitatively attribute the changes in streamflow. The basin's evolutionary trajectory in the Budyko space is shown in Fig. 7 (a). The Budyko analysis, based on a calibrated catchment parameter (n) of 1.776, quantitatively confirms the dominant role of human activities in altering the basin's hydrology, particularly during the period of intensive intervention. From the baseline period (P1) to the period of intensive alteration (P2), the total observed runoff decreased by 0.31 km³/yr. Our attribution results are unequivocal: direct human activities were the overwhelming driver of this decline, accounting for -0.27 km³/yr, or 86.3% of the total change. Remarkably, this occurred while the climate became slightly less arid (aridity index, ϕ, decreased from 1.404 to 1.349). This finding underscores that the significant hydrological deficit during this era was not a consequence of adverse climate conditions but was almost entirely driven by anthropogenic water withdrawals, consistent with the reality of large-scale water storage at the Kapchagay Reservoir.~~

Formatted: Font: (Default) +Headings (Times New Roman), (Asian) 宋体, English (United Kingdom)

Formatted: Indent: First line: 2 ch, Don't adjust right indent when grid is defined, Don't snap to grid

Formatted: Font: (Default) +Headings (Times New Roman)

Formatted: Font: (Default) +Headings (Times New Roman)

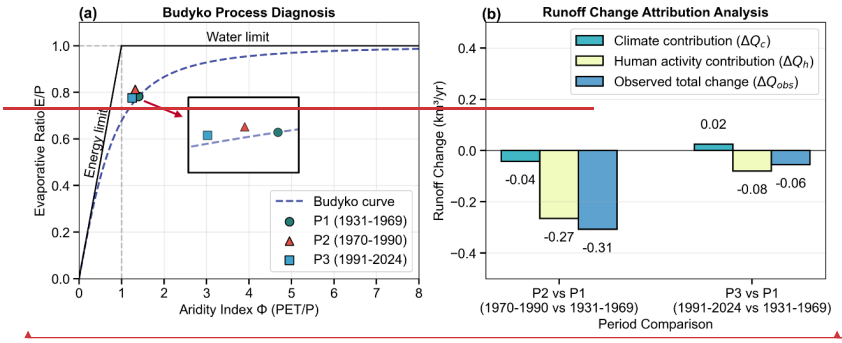

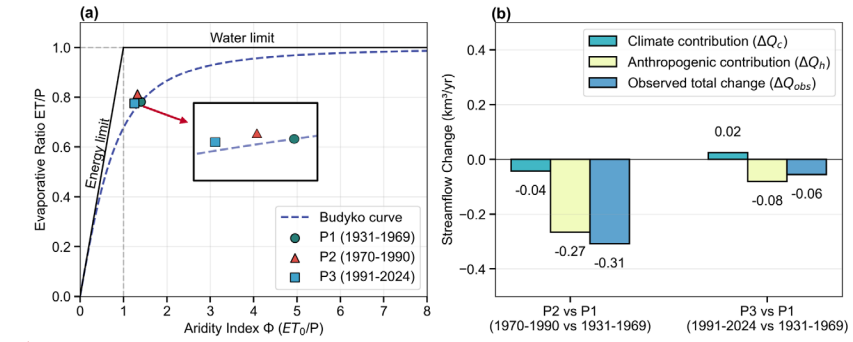

Figure ~~7~~ 8. Budyko analysis ~~and attribution~~ of streamflow~~runoff~~ changes. (a) Trajectory of the basin's hydro-climatic conditions across three periods. (b) Contribution~~Attribution~~ of total streamflow~~runoff~~ changes between periods to climate and human activity contributions

In the subsequent period (P3), the dynamic between drivers shifted. Observed streamflow nearly recovered to baseline levels (a minor change of -0.06 km³/yr), but this apparent stability obscures underlying competing forces. The climate trend alone would have led to a modest increase in streamflow (+0.02 km³/yr) due to a continued shift toward less arid conditions (ϕ = 1.287). However, this potential climatic gain was offset by the persistent negative impact of human activities (-0.08 km³/yr). This analysis highlights a crucial transition: while the absolute magnitude of human impact lessened compared to P2, it remained sufficient to counteract the favorable climate trend, preventing full hydrological recovery. The system has thus evolved from one dominated by direct human intervention to one where human water use suppresses the benefits of a wetter climate cycle.

A detailed contribution analysis, decomposing the climatic signal into its constituent parts, reveals significant compensating effects among the drivers (Table 3). During the intensive alteration period (P2 vs. P1), climatic factors alone would have

Formatted: Font: (Default) +Headings (Times New Roman)
Formatted: Font: (Default) +Headings (Times New Roman), 10 pt
Formatted: Font: (Default) +Headings (Times New Roman)
Formatted: Font: (Default) +Headings (Times New Roman), 10 pt
Formatted: Font: (Default) +Headings (Times New Roman)

resulted in a substantial increase in streamflow (+6.13 km³). This counter-intuitive result was driven by a marked decrease in ET_0), which contributed +19.50 km³ to streamflow, largely compensating for the decline in glacial melt (-13.71 km³). However, this climatic gain was negated by the substantial impact of direct human activities, which caused a -9.21 km³ reduction in flow. This demonstrates that the observed moderate decline in streamflow was the net result of a climate-driven water surplus being offset by anthropogenic withdrawals.

This pattern of opposing forces intensified in the most recent period (P3 vs. P1). The climate-driven potential for streamflow generation increased to +10.80 km³, driven primarily by a continued decrease in ET_0 (+17.38 km³) and increased rainfall (+10.41 km³). These gains were sufficient to offset the continued decline in glacial melt (-16.64 km³). Yet, despite this potential for a wetter regime, observed streamflow remained near baseline levels because the negative impact of human activities also intensified (-11.36 km³), effectively neutralizing the climate-driven surplus. These findings suggest a delicate hydrological balance: the basin's apparent stability is maintained by the opposition of substantial competing forces. A shift in this balance—such as a reversal in ET_0 trends or a decrease in rainfall—could expose the system to the full impact of reduced cryospheric storage and sustained human water demand.

~~In the subsequent period (P3), the dynamic between drivers shifted dramatically. The observed runoff nearly recovered to baseline levels (a minor change of -0.06 km³/yr), but this apparent stability masks a critical dynamic of competing forces. The climate trend, on its own, would have led to a modest increase in runoff (+0.02 km³/yr) due to a continued shift toward less arid conditions (ϕ = 1.287). However, this potential climatic gain was entirely offset and surpassed by the persistent negative impact of human activities (-0.08 km³/yr). This analysis highlights a crucial transition: while the absolute magnitude of human impact lessened compared to P2, it remained strong enough to counteract a favorable climate trend, preventing a full hydrological recovery. The system has thus evolved from one dominated by direct human intervention to one where human water use actively suppresses the benefits of a wetter climate cycle.~~

~~A detailed attribution analysis, which decomposes the climatic contribution into its constituent parts, reveals a powerful but hidden dynamic of competing forces that have fundamentally reshaped the basin's hydrology (Table 2). During the period of intensive alteration (P2 vs. P1), the climate, on its own, would have caused a massive increase in runoff, calculated at +6.13 km³. This seemingly paradoxical result was driven by a very large decrease in potential evapotranspiration (PET), which contributed +19.50 km³ to runoff, overwhelmingly compensating for the severe decline in glacial melt (-13.71 km³). However, this substantial climatic gain was entirely erased by the immense impact of direct human activities, which caused a -9.21 km³ reduction in flow. This demonstrates that the observed moderate decline in runoff was the net result of a massive climate-driven water surplus being entirely offset by equally massive anthropogenic withdrawals.~~

Table 3. ~~Decomposition of Climate and Human Impacts on Runoff~~Decomposition of Climate and Human Contributions to Inflow Changes

	P2 vs P1			
Component	Δx_i	$\partial Q/\partial x$	ΔQ_i	$\Delta Q_i/\Delta Q$(%)

Formatted: Font: (Default) +Headings (Times New Roman)

Formatted: Font: (Default) +Headings (Times New Roman)

Formatted: Font: (Default) +Headings (Times New Roman)

Formatted: Font: (Default) +Headings (Times New Roman), 10 pt

Rain	0.674	1.335	0.899	-29.2
$Melt_{snow}$	-0.421	1.335	-0.562	18.3
$Melt_{glacier}$	-10.270	1.335	-13.709	445.4
~~P~~ET_0	-18.153	-1.074	19.500	-633.5
n	/	/	-9.206	299.1

Component	P3 vs P1 Δx_i	$\partial Q/\partial x$	ΔQ_i	$\Delta Q_i/\Delta Q(\%)$
Rain	7.801	1.335	10.414	-187.5
$Melt_{snow}$	-0.264	1.335	-0.352	63.4
$Melt_{glacier}$	-12.468	1.335	-16.643	299.7
~~P~~ET_0	-16.183	-1.074	17.384	-313.0
n	/	/	-11.358	204.52

~~This pattern of opposing forces intensified dramatically in the most recent period (P3 vs. P1). The climate-driven potential for runoff generation soared to +10.80 km³, again fueled primarily by a large decrease in PET (+17.38 km³) and a significant increase in rainfall (+10.41 km³). These gains were more than enough to offset the continued and worsening decline in glacial melt (-16.64 km³). Yet, despite this enormous climatic potential for a wetter regime, the observed runoff remained near baseline levels. This was because the negative impact of human activities also intensified to -11.36 km³, effectively neutralizing the entire climate-driven surplus. These findings expose a critical vulnerability: the basin's apparent hydrological stability is a fragile illusion, maintained only by a coincidental and likely temporary opposition of very large, opposing forces. Any change in this delicate balance—such as a return of PET to higher levels or a decrease in rainfall—could expose the system to the full, severe impact of its lost cryospheric storage and sustained human water demand.~~

Formatted: Subscript

Formatted: Subscript

Formatted: Font: (Default) +Headings (Times New Roman), 10 pt, Font color: Auto

Formatted: Font: (Default) +Headings (Times New Roman)

3.3 Lake System Response to Changes in Water Supply

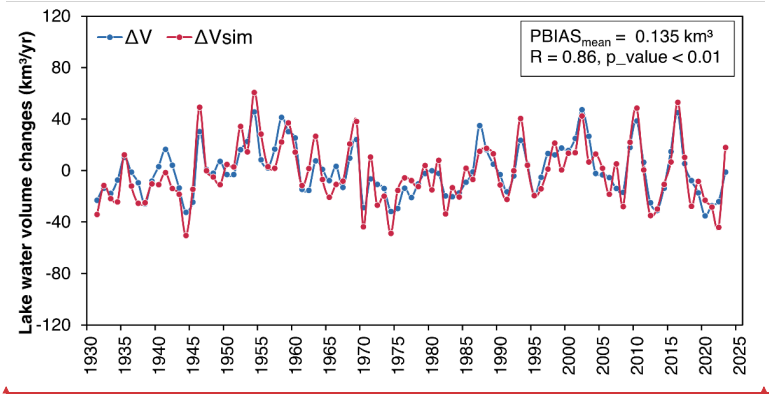

Figure ~~8~~ 9. Comparison of simulated annual lake volume changes (ΔV_s) versus reconstructed volume changes derived from observed lake levels and areas (ΔV_{sim})~~simulated water volume changes and water volume changes calculated based on lake data~~

To provide a final, integrated validation of the modeling framework, we compared the reconstructed annual lake water volume changes (ΔV_s) with the simulated volume changes (ΔV_{sim}). The reconstructed ΔV_s was derived from satellite-based water level and area data, representing the observed variations in lake storage. The simulated ΔV_{sim} was calculated independently as the net result of modeled total inflow minus lake surface evaporation. As shown in Fig. 9, there is a strong correspondence between the two time series, with the model successfully capturing the magnitude and timing of major inter-annual fluctuations. This agreement is substantiated by robust statistical metrics: the correlation coefficient (R) is 0.86 ($p<0.01$), indicating a highly significant positive relationship, and the mean bias is low at 0.135 km³/yr. This cross-validation confirms that the framework accurately closes the water balance at the lake terminus. Since the simulated volume change is directly dependent on the accuracy of reconstructed inflow, this result provides high confidence in the reliability of the streamflow data used for the subsequent contribution analysis. To provide further climatic context, it is noted that the basin has experienced a significant warming trend over the study period (1931-2024), with mean annual temperatures increasing by approximately 0.30 °C/decade ($p<0.001$), a factor that fundamentally influences the evaporative dynamics discussed below.

The dynamic reconstruction of the Lake Balkhash water balance, illustrated in Fig. 10, reveals significant variability driven primarily by fluctuations in river inflow. During the Reference Period (P1), the lake existed in a state of relative equilibrium. Mean annual inflow of 18.4 km³/yr was nearly balanced by lake surface evaporation of 20.4 km³/yr, resulting in a negligible mean ΔV_s of +0.07 km³/yr. The lake experienced years of water gain and loss in roughly equal measures (46% vs. 54%). This stability was abruptly disrupted in the Intensive Intervention Period (P2). A sharp decline in mean annual inflow to 15.3 km³/yr—a drop of over 3 km³/yr—shifted the system into a state of sustained deficit. Despite a concurrent decrease in

Formatted: Font: (Default) +Headings (Times New Roman)
Formatted: Font: (Default) +Headings (Times New Roman), 10 pt
Formatted: Font: 10 pt
Formatted: Font: (Default) +Headings (Times New Roman), 10 pt
Formatted: Font: 10 pt
Formatted: Font: 10 pt
Formatted: Font: 10 pt
Formatted: Font: (Default) +Headings (Times New Roman), 10 pt
Formatted: Font: (Default) +Headings (Times New Roman)
Formatted: Font: (Default) +Headings (Times New Roman)
Formatted: Font: (Default) +Headings (Times New Roman)
Formatted: Font: (Default) +Headings (Times New Roman)
Formatted: Font: (Default) +Headings (Times New Roman)
Formatted: Font: (Default) +Headings (Times New Roman)

evaporation, the reduced input was significant; consequently, lake storage declined by an average of 1.0 km³/yr, with two-thirds of the years in this period experiencing a net water loss, leading to a cumulative volume reduction of 21.0 km³.

~~To provide a final, integrated validation of our entire modeling framework, we compared the reconstructed annual lake water volume changes (ΔV) with the simulated volume changes (ΔVsim). The reconstructed ΔV was derived from satellite-based water level and area data, representing the observed reality of the lake's storage change. The simulated ΔV_{sim} was calculated independently as the net result of our modeled total inflow minus lake surface evaporation. As shown in Fig. 8, there is a strong visual correspondence between the two time series, with the model successfully capturing the magnitude and timing of the major inter-annual fluctuations. This visual agreement is substantiated by robust statistical metrics: the correlation coefficient (R) is 0.86 ($p < 0.01$), indicating a highly significant positive relationship, and the mean bias is exceptionally low at 0.135 km³/yr. This strong agreement serves as a crucial cross-validation, confirming that our framework accurately closes the water balance at the lake terminus. Since the simulated volume change is directly dependent on the accuracy of our reconstructed inflow, this result provides high confidence in the reliability of the runoff data used for the subsequent attribution analysis.~~

~~The dynamic reconstruction of the Lake Balkhash water balance, illustrated in Fig. 9, reveals a dramatic history of change driven primarily by fluctuations in river inflow. During P1, the lake existed in a state of relative equilibrium. Mean annual inflow of 18.4 km³/yr was nearly balanced by lake surface evaporation of 20.4 km³/yr, resulting in a negligible mean storage change (ΔV) of +0.07 km³/yr. The lake experienced years of water gain and loss in roughly equal measures (46% vs. 54%). This stability was abruptly shattered in the P2. A sharp decline in mean annual inflow to 15.3 km³/yr, a drop of over 3 km³/yr, directly tipping the balance into a state of sustained deficit. Despite a concurrent decrease in evaporation, the reduced input was so significant that the lake's storage declined by an average of 1.0 km³/yr, with two-thirds of the years in this period experiencing a net water loss and a cumulative volume reduction of 21.0 km3.~~

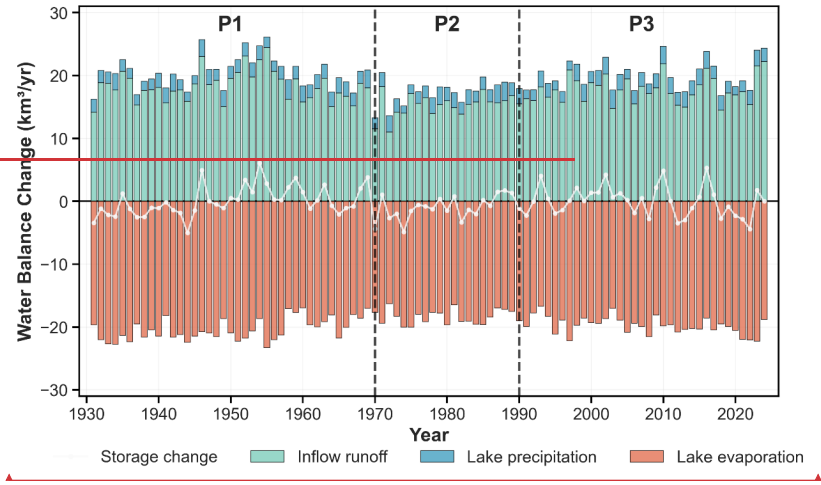

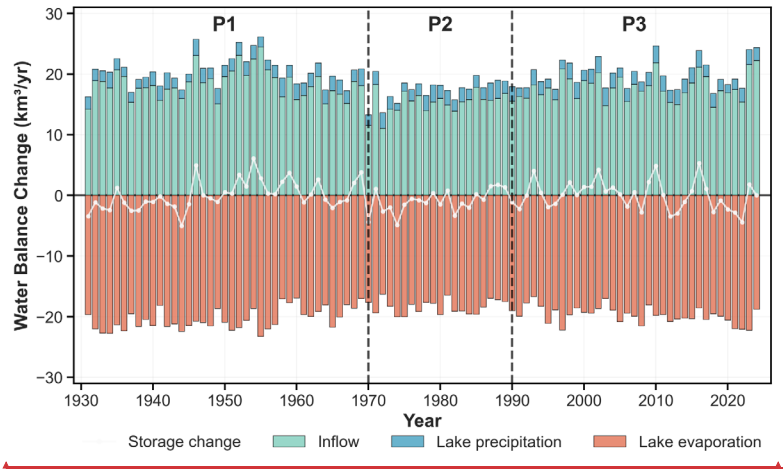

Figure ~~9~~ 10.~~Long-term water balance of Lake Balkhash~~ Long-term water balance components of Lake Balkhash (1931-2024), showing Inflow, Evaporation, and Net Storage Change.

The Compounded Pressures Period (P3) marked a phase of partial recovery and re-stabilization. Inflow rebounded to 17.8 km³/yr, approaching pre-1970 levels. This recovery in water supply was sufficient to counteract evaporative losses (19.8 km³/yr), bringing the mean storage change back to a near-neutral state (+0.04 km³/yr) and restoring a positive water balance

Formatted: Font: (Default) +Headings (Times New Roman)

Formatted: Font: (Default) +Headings (Times New Roman), 10 pt

Formatted: Font: (Default) +Headings (Times New Roman)

Formatted: Font: (Default) +Headings (Times New Roman), 10 pt

Formatted: Font: (Default) +Headings (Times New Roman)

in a majority of years (55.9%). A notable finding is the statistically significant, albeit slight, decreasing trend in total lake surface evaporation over the entire 1931-2024 period ($p<0.05$). This suggests that despite a warming climate, other factors such as changes in wind speed, humidity, or lake surface thermal dynamics may have modulated long-term open-water evaporation. Across all periods, river inflow consistently accounted for ~90% of the total water input, identifying it as the primary driver controlling the lake's state. The lake's storage volume is thus highly sensitive to the marginal difference between these large input and output fluxes. The ~17% reduction in inflow during P2 was sufficient to trigger a prolonged period of decline, while its subsequent recovery was the key factor in the lake's recent stabilization. This highlights the critical dependence of the lake ecosystem on catchment hydrological processes.

To synthesize these findings into a comprehensive explanation for the lake's historical trajectory, we performed a final contribution analysis on the changes in mean annual lake water storage (Fig. 11). During the intensive alteration period (P2 vs. P1), the lake's water balance improved relative to the baseline, with the mean storage change increasing by +4.54 km^3. This was driven by a substantial positive climatic contribution of +7.17 km^3, primarily caused by the reduction in lake surface evaporation. However, this climatic benefit was simultaneously counteracted by the negative impact of direct human activities (-2.63 km^3), which consumed more than a third of the potential gain through reduced inflow. This reveals that the lake's water balance was maintained largely due to favorable climatic conditions, despite the anthropogenic pressures of that era.

This dynamic of opposing forces became even more pronounced in the most recent period (P3 vs. P1). The positive climatic contribution increased to +12.49 km^3, fueled by both a continued decrease in evaporation and a substantial increase in direct precipitation over the lake. While the negative impact of human activities persisted (-0.87 km^3), it was exceeded by the magnitude of the favorable climate trend, resulting in a large net increase in the lake's storage change of +11.62 km^3. Ultimately, these results provide a critical insight: the apparent hydrological stability and recent recovery of Lake Balkhash are not indicative of intrinsic resilience but are instead delicately balanced and supported by a highly favorable climatic trend. The underlying water deficit caused by human use remains, offset only by these favorable conditions. Any reversal in these climatic trends could rapidly expose the lake's vulnerability.

~~The P3 marked a phase of partial recovery and re-stabilization. Inflow rebounded significantly to 17.8 km^3/yr, approaching pre-1970 levels. This recovery in water supply was sufficient to counteract the evaporative losses (19.8 km^3/yr), bringing the mean storage change back to a near-neutral state (+0.04 km^3/yr) and restoring a majority of years (55.9%) to a positive water balance. A noteworthy and perhaps counter-intuitive finding is the statistically significant, albeit slight, decreasing trend in total lake surface evaporation over the entire 1931-2024 period ($p < 0.05$). This suggests that despite a warming climate, other factors such as changes in wind speed, humidity, or lake surface thermal dynamics may have modulated and even slightly reduced long-term open-water evaporation. Across all periods, river inflow consistently accounted for ~90% of the total water input, making it the primary lever controlling the lake's state. The lake's storage volume, and by extension its water level, is thus extremely sensitive to the marginal difference between these massive inputs and outputs. The ~17% reduction in inflow during P2 was sufficient to trigger a prolonged period of decline, while its subsequent recovery was the key factor in the lake's recent stabilization. This highlights the critical dependence of this vital ecosystem on the hydrological health of its catchment.~~

To synthesize our findings into a comprehensive explanation for the lake's historical trajectory, we performed a final attribution analysis on the changes in the mean annual lake water storage, with the results presented in Fig. 10. During the intensive alteration period (P2 vs. P1), the lake's water balance paradoxically improved, with the mean storage change increasing by a substantial +4.54 km³. This was driven by a powerful, positive climatic contribution of +7.17 km³, primarily caused by a significant reduction in lake surface evaporation. However, this massive climatic benefit was simultaneously counteracted by the negative impact of direct human activities (-2.63 km³), which, through reduced inflow, consumed more than a third of the potential gain. This reveals that the lake's water balance improved despite, not because of, the anthropogenic pressures of that era.

This dynamic of opposing forces became even more pronounced in the most recent period (P3 vs. P1). The positive climatic contribution soared to an immense +12.49 km³, fueled by both a continued decrease in evaporation and a substantial increase in direct precipitation over the lake. While the negative impact of human activities persisted (-0.87 km³), it was dwarfed by the magnitude of the favorable climate trend, resulting in a large net increase in the lake's storage change of +11.62 km³. Ultimately, these results provide a critical insight: the apparent hydrological stability and recovery of Lake Balkhash are not a sign of intrinsic resilience but are instead precariously balanced and heavily subsidized by a highly favorable, and potentially transient, climatic trend. The persistent underlying water deficit caused by human use remains, masked by this climatic boon. Any reversal of these favorable climate conditions could rapidly expose the lake's profound vulnerability.

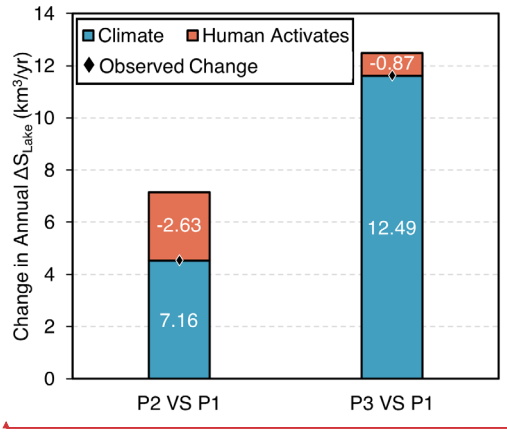

Formatted: Font: (Default) +Headings (Times New Roman)

Formatted: Font: (Default) +Headings (Times New Roman), 10 pt

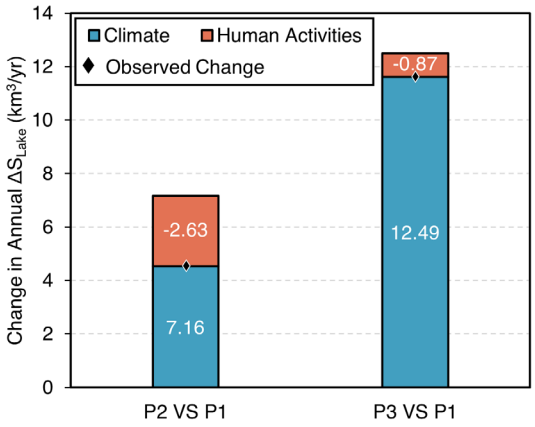

Figure ~~10~~ 11. ~~Attribution of changes in Lake Balkhash water Storage~~Quantitative contribution analysis of drivers (Climate vs. Human Activity) to changes in Lake Balkhash water storage relative to the baseline period (P1).

3.4 Changes in Lake Water Levels Under Future Scenarios

~~4. Discussion~~

~~This study successfully introduced and implemented a novel attribution framework to disentangle the complex, century-long interplay between climate change and human activities on the hydrology of the Lake Balkhash basin. Our results not only quantifying the drivers of streamflow change but also by explicitly linking these changes to the lake's ultimate water balance response. A key finding is that the basin's hydrology has been shaped by a powerful, and often counter-intuitive, dynamic of large, opposing forces. While previous research has correctly identified the Kapchagay Reservoir's impoundment as the primary cause of the lake's decline in the 1970s and 80s (Duan et al., 2021; Kezer & Matsuyama, 2006), our detailed attribution provides a more nuanced understanding. We demonstrate that this human-induced water withdrawal was so immense (-9.21 km³) that it completely masked a significant, climate-driven potential for a wetter regime (+6.13 km³), a phenomenon largely overlooked in prior assessments. This finding underscores that the era's ecological crisis was even more severe than the observed runoff decline alone would suggest, as it unfolded against a favorable climatic backdrop.~~

~~The most recent period (post-1991) reveals a critical evolution in the basin's vulnerability. Our analysis shows that while direct human impact has lessened, the basin's apparent stability is heavily subsidized by an exceptionally favorable climatic trend, characterized by increased rainfall and decreased potential evapotranspiration. This aligns with recent findings of increasing precipitation in parts of Central Asia (Jin et al., 2024), but our study is the first to quantify how this "climatic boon" (+10.80 km³) has been almost entirely neutralized by ongoing human water use (-11.36 km³). This exposes a fragile equilibrium: the~~

Formatted: Font: (Default) +Headings (Times New Roman)

Formatted: Font: (Default) +Headings (Times New Roman), 10 pt

Formatted: Font: (Default) +Headings (Times New Roman)

Formatted: Font: (Default) +Headings (Times New Roman), Font color: Auto

Formatted: Font: (Default) +Headings (Times New Roman)

~~current stability of Lake Balkhash is not a sign of intrinsic resilience or successful water management, but rather a coincidental and likely temporary stalemate between massive, opposing forces. This finding challenges the narrative of a simple "recovery" and instead highlights a state of heightened, masked vulnerability. Any future reversal of the recent favorable precipitation or PET trends could rapidly expose the system to the full, unbuffered impact of this lost storage and sustained human demand.~~

~~To further probe the precarious equilibrium identified in Period 3 and to underscore the system's vulnerability, we extended our integrated modeling framework to project future changes in Lake Balkhash's water level through 2100 under three distinct Shared Socioeconomic Pathways (SSPs): a low-emissions sustainability scenario (SSP1-2.6), a medium-high emissions scenario (SSP3-7.0), and a very high-emissions, fossil-fueled development scenario (SSP5-8.5). Parameters were referenced from P3, and climate-driven data were obtained from NEX-GDDP-CMIP6. To simulate future land-use changes, we referenced the research of~~

To probe the sustainability of the current hydrological equilibrium and assess future vulnerabilities, we extended the integrated modeling framework to project Lake Balkhash's water level trajectory through 2100. Projections were driven by three Shared Socioeconomic Pathways (SSPs) from the NEX-GDDP-CMIP6 dataset: a low-emissions sustainability scenario (SSP1-2.6), a medium-high emissions scenario (SSP3-7.0), and a fossil-fueled development scenario (SSP5-8.5). Future land-use changes were simulated based on the expansion trends observed over the past two decades, capped at a maximum expansion of 15% following the methodology of ~~(Guo et al., 2015),~~ Guo et al. (2015). Catchment parameters were referenced from the calibrated Period 3 (P3) set to represent current management baselines.~~simulating future land-use conditions based on the land expansion rate over the past 20 years and the maximum expansion condition of 15%.~~

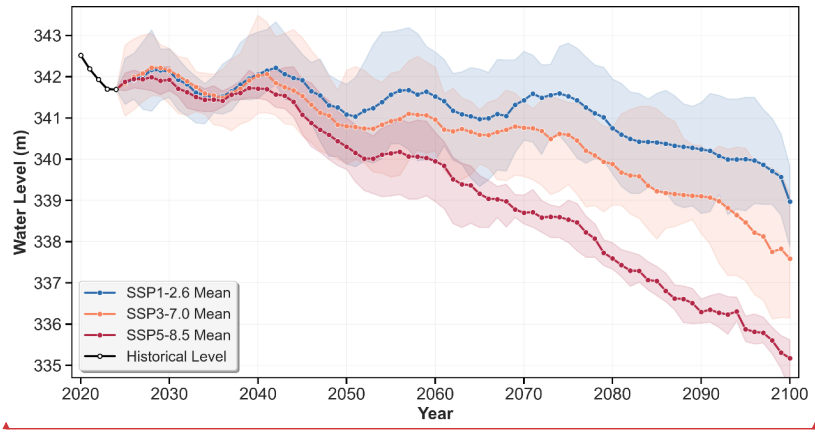

**Figure ~~11~~ 12. ~~C~~Projected changes in Lake Balkhash water levels (2025–2100) under three Shared Socioeconomic Pathways (SSPs). The horizontal dashed line indicates the critical historical low level (340.52 m).~~hanges in lake water levels under three future scenarios~~

Formatted: Font: (Default) +Headings (Times New Roman)

Formatted: Font: (Default) +Headings (Times New Roman)

Formatted: Font: (Default) +Headings (Times New Roman)

Formatted: Font: (Default) +Headings (Times New Roman), 10 pt

~~The results as depicted in Fig. 11, reveal a concerning trajectory across all considered futures, unequivocally demonstrating that the apparent stability of the late 20th and early 21st centuries is a fragile and transient condition. Under the most optimistic scenario (SSP1-2.6), Lake Balkhash is projected to experience a slow but steady decline, with its water level falling by approximately 2.5 meters from its 2020 level by 2100. This indicates that even with aggressive global climate mitigation, the combined pressures of existing human water demand and the legacy of cryospheric decline will likely overwhelm the system's resilience. In stark contrast, the medium-to-high-emissions scenarios (SSP3-7.0 and SSP5-8.5) portend a much more severe fate. Under these pathways, the lake experiences a pronounced and accelerated decline, particularly after 2040s. Historically, the lowest water level of Lake Balkhash was 340.52 meters, a period marked by severe ecological conditions. Under the medium emissions scenario, this water level would be reached by the 2070s of this century, while under the high emissions scenario, it would occur as early as the 2050s of this century. These scenarios starkly illustrate that the "climatic boon" of increased precipitation and reduced PET that subsidized the lake's water balance in recent decades is not guaranteed to continue. As this favorable climatic trend wanes or reverses under future warming, the persistent and powerful negative impacts of human water demand and the systematic loss of glacial storage—previously masked—are set to become the dominant drivers, precipitating a rapid contraction of the lake. These future projections confirm our central finding: the current state of Lake Balkhash is not one of recovery, but of a masked vulnerability, sustained by a temporary climatic subsidy that is highly likely to diminish, exposing the ecosystem to severe and potentially irreversible consequences.~~

The projections, depicted in Fig. 12, reveal a concerning trajectory across all considered scenarios, suggesting that the stability observed in the late 20th and early 21st centuries may be transient. Under the optimistic SSP1-2.6 scenario, which assumes aggressive climate mitigation, the lake is projected to experience a gradual but steady decline, with water levels falling by approximately 2.5 meters relative to the 2020 baseline by 2100. This indicates that current human water demands, combined with the legacy effects of cryospheric depletion, may override the system's resilience even in the absence of severe future warming. In contrast, the medium-to-high emissions scenarios (SSP3-7.0 and SSP5-8.5) portray a significantly more severe outcome, characterized by an accelerated decline particularly after the 2040s. A critical threshold is the historical low water level of 340.52 m, a benchmark previously associated with severe ecological degradation. Our model indicates this threshold would be breached by the 2070s under SSP3-7.0 and as early as the 2050s under SSP5-8.5. While these projections do not suggest complete desiccation by 2100, the magnitude of the decline—exceeding 2 to 4 meters—implies a high risk of morphological fragmentation and ecological collapse, illustrating that the "climatic subsidy" currently supporting the lake is insufficient to counteract the intensifying pressures of future warming and sustained human demand.

While the projections do not indicate that the lake will completely dry up by 2100 (water levels remain above the lake bed elevation in the deeper eastern basin), the magnitude of the decline suggests a high risk of ecological collapse and morphological fragmentation. The projected drop of over 2-4 meters would likely lead to the separation of the western (fresh) and eastern (saline) basins, severe salinization, and the exposure of vast areas of the lake bed, mirroring the trajectory of the Aral Sea. These scenarios illustrate that the favorable climatic conditions (increased precipitation and reduced ET_a) that have supported the lake in recent decades are insufficient to counteract the intensifying evapotranspiration and sustained human

Formatted: Font: (Default) +Headings (Times New Roman)

Formatted: Font: (Default) +Headings (Times New Roman)

demand expected under higher warming trajectories. The "climatic subsidy" is likely to diminish, allowing the persistent water deficit to become the dominant driver of a rapid lake contraction.

4. Discussion

4.1 Mechanisms of Historical Change: The "Masking Effect" of Climate

The application of the HADF has revealed a critical, previously underappreciated dynamic in the Lake Balkhash basin: the hydrological system is defined by the competition between substantial, opposing forces. While previous studies have correctly identified the impoundment of the Kapchagay Reservoir and agricultural expansion as the primary drivers of the lake's decline in the 1970s and 1980s (Duan et al., 2020; Kezer and Matsuyama, 2006)———, our component-level analysis offers a more nuanced quantitative understanding. We demonstrate that the human-induced water withdrawal during the Intensive Intervention Period (P2) was of such magnitude (-9.21 km³) that it completely masked a significant, climate-driven potential for a wetter regime (+6.13 km³). This finding is crucial because it implies that the ecological crisis of that era occurred against a paradoxically favorable climatic backdrop. Had the climate been stationary or drier, the lake's contraction would likely have been catastrophic, mirroring the fate of the Aral Sea much earlier.

This "masking effect" has evolved in the post-1991 period (P3) into a state of "subsidized stability." Our results align with recent evidence of a "wetting" trend in Central Asia, characterized by increased precipitation and accelerated cryospheric melt (Jin et al., 2024; Zhang et al., 2021). However, unlike previous assessments that viewed the recent lake level recovery as a sign of successful management or resilience (Zhao et al., 2025), our study quantifies that this positive climatic contribution (+10.80 km³) has been almost entirely neutralized by ongoing, and even intensifying, human water use (-11.36 km³). This exposes a delicate equilibrium: the current stability is not intrinsic but is maintained by a stalemate between large fluxes. This distinction is vital for policy-making; it suggests that the basin has no buffer. Any reversal in the favorable precipitation trend—or the inevitable decline in glacial melt contribution—would rapidly expose the system to the unbuffered impact of sustained human demand.

4.2 Cryospheric Dynamics and Methodological Limitations

A critical methodological challenge in hydrological reconstruction, particularly in high-mountain Asia, is the assumption of stationary catchment properties. In our "Naturalized Inflow" simulation, we applied the parameter set calibrated for the baseline period (1931-1969) to the entire study period. As noted by the reviewers, this approach assumes that the glacio-hydrological response characteristics (e.g., glacier area, melt efficiency) remained constant, whereas in reality, the region has warmed significantly (Section 3.3).

This assumption has important implications for our attribution results. The baseline parameters reflect the cryospheric conditions of the mid-20th century, when glacier volumes were larger. Applying these parameters to the warmer, recent

Formatted: Font: (Default) +Headings (Times New Roman), Font color: Auto
Formatted: Font: (Default) +Headings (Times New Roman)
Formatted: Heading 2
Formatted: Font: (Default) +Headings (Times New Roman)
Formatted: Font: (Default) +Headings (Times New Roman)
Formatted: Font: (Default) +Headings (Times New Roman)
Formatted: Font: (Default) +Headings (Times New Roman)
Formatted: Font: (Default) +Headings (Times New Roman)

decades likely results in a simulation of "natural" runoff that captures the climatic drivers (precipitation and temperature) but may not fully capture the dynamic transient response of accelerating glacier mass loss (the "glacier surplus" effect) or the changing area-volume scaling. Recent studies suggest that many Central Asian catchments are currently in a phase where accelerated melt from retreating glaciers temporarily boosts runoff (Peak Water) (Huss and Hock, 2018; Sorg et al., 2012). By using static parameters, our Q_{nat} might underestimate this transient meltwater bonus.

However, this limitation essentially renders our attribution of human impact conservative. If the "true" natural runoff (accounting for accelerated melt) was even higher than our simulated Q_{nat}, then the gap between natural supply and Q_{act} would be even larger. This means that the actual volume of water withdrawn by human activities is likely greater than our calculated estimates. Therefore, while we acknowledge the uncertainty introduced by the stationary parameter assumption, it reinforces rather than weakens our central conclusion: human activities are the dominant force suppressing the basin's water availability, potentially consuming not just the renewable precipitation but also the non-renewable glacial storage. Future research integrating dynamic glacier evolution models (e.g., GloGEM) into hydrological frameworks is essential to explicitly quantify this "fossil water" component.

~~While HAAF framework demonstrated robust performance and provided novel insights, certain limitations and uncertainties should be acknowledged. First, the Budyko framework, despite its strengths, simplifies complex landscape processes into a single parameter (n). The positive contribution attributed to "human activity" (the Δn term) in our component analysis likely captures complex, secondary land-surface feedbacks (e.g., irrigation return flows, land use changes) that are difficult to disentangle from the primary impact of direct water withdrawal. Future work could employ more process-detailed models or isotopic tracers to further partition these human impacts. Second, although we used the highest-quality, long-term datasets available, uncertainties persist in historical meteorological forcings and reconstructed naturalized flows, particularly in the early 20th century. Our integrated validation of the lake's water balance provides strong confidence in our overall results, but continued efforts to improve historical data rescue and reconstruction are vital.~~

4.3 Future Vulnerabilities and Uncertainties

The projections presented in Section 3.4 highlight a concerning trajectory for Lake Balkhash, yet these findings must be interpreted within the context of inherent uncertainties. The primary source of uncertainty stems from the GCM projections themselves. While we utilized an ensemble of six high-performing CMIP6 models to mitigate individual biases, future precipitation changes in Central Asia remain notoriously difficult to predict, with significant inter-model spread (Mishra et al., 2024). A second critical uncertainty concerns the timing of "peak water" from glacial melt. Our hydrological simulations implicitly rely on temperature-melt relationships; however, as glacier volume diminishes, the meltwater contribution will inevitably decline regardless of rising temperatures (Huss and Hock, 2018). If the Ili River basin crosses this tipping point sooner than anticipated (e.g., by mid-century), the decline in inflow under SSP3-7.0 and SSP5-8.5 could be significantly sharper and more abrupt than our current linear projections suggest. Furthermore, our projections assume that future land use will follow historical expansion trends (Guo et al., 2015). This "business-as-usual" assumption does not account for potential

Formatted: Font: (Default) +Headings (Times New Roman)
Formatted: Font: (Default) +Headings (Times New Roman)
Formatted: Font: (Default) +Headings (Times New Roman)
Formatted: Font: (Default) +Headings (Times New Roman)
Formatted: Font: (Default) +Headings (Times New Roman)
Formatted: Font: (Default) +Headings (Times New Roman)
Formatted: Font: (Default) +Headings (Times New Roman)
Formatted: Font: (Default) +Headings (Times New Roman)
Formatted: Font: (Default) +Headings (Times New Roman)
Formatted: Font: (Default) +Headings (Times New Roman)
Formatted: Font: (Default) +Headings (Times New Roman)

adaptive measures, such as improvements in irrigation efficiency (e.g., drip irrigation) or shifts to less water-intensive crops, nor does it factor in the possibility of aggressive agricultural expansion driven by regional food security needs. These factors collectively suggest that while the direction of change is clear, the specific rate and magnitude of the lake's decline could vary based on the interplay of these complex climatic and socioeconomic dynamics.

Despite these uncertainties, the signal across all scenarios is consistent: the "climatic subsidy" is transient. The current favorable water balance relies heavily on increased inputs (rainfall + melt). As the melt component inevitably wanes and evapotranspiration demand rises with temperature, the "masking effect" will fade. This will leave the lake exposed to the full weight of human water consumption, likely precipitating a rapid hydrological contraction and ecological degradation similar to the Aral Sea disaster, but potentially faster due to the shallower nature of Lake Balkhash.

5. Conclusion

This study developed and implemented the Hydrological Analysis and Disentanglement Framework (HADF), integrating hybrid hydrological models with the Budyko framework and a lake water balance model, to quantitatively separate the contributions of climate change and human activities to the centennial hydrology of the Lake Balkhash basin. Our primary objective was to provide a comprehensive, quantitative explanation for the lake's historical water level dynamics by tracing the drivers of change from the catchment to the lake terminus. Our key findings are as follows:

(1) High-Fidelity Reconstruction: The HADF successfully reconstructed both naturalized and actual streamflow with high accuracy (KGE > 0.75, |PBIAS| < 10% for most stations), establishing a robust foundation for contribution analysis. The final integrated validation confirmed that the framework accurately closes the lake's water balance, with simulated volume changes exhibiting a strong correlation with satellite-derived observations (R=0.86).

(2) Dynamics of Opposing Forces: At the catchment scale, the analysis of runoff changes revealed a dynamic interaction between substantial, opposing forces. During the Intensive Intervention Period (1970–1990), direct human activities were the dominant driver of runoff decline, accounting for a reduction of -9.21 km³. This substantial anthropogenic pressure effectively masked a significant climate-driven potential for a wetter regime (+6.13 km³). Subsequently, during the recent period (1991–2024), the basin's hydrology entered a state of delicate equilibrium, where a large climate-driven potential for runoff increase (+10.80 km³) was almost entirely counteracted by the sustained impact of human water use (-11.36 km³).

(3) Lake Response and Future Vulnerability: These catchment-scale dynamics directly governed the lake's response. The apparent stability of Lake Balkhash in recent decades was not indicative of intrinsic resilience but was supported by a highly favorable climatic trend that buffered the system against persistent anthropogenic water stress. However, our future projections under multiple SSP scenarios indicate that this climatic buffer is likely transient. As these favorable conditions wane or reverse, the underlying pressures from human activities and cryospheric decline are projected to dominate, potentially leading to a rapid and significant decline in lake water levels. This demonstrates that the current equilibrium is precarious and obscures a significant long-term vulnerability.

Formatted: Font: (Default) +Headings (Times New Roman), Font color: Auto

Formatted: Font: (Default) +Headings (Times New Roman)

In conclusion, our research reveals that the recent stability of Lake Balkhash represents a state of "masked vulnerability," sustained by favorable but likely temporary climatic conditions rather than systemic recovery. This study underscores the critical need for transboundary water management strategies that look beyond short-term trends and account for the underlying, competing drivers of the system. The framework presented here provides a robust tool for diagnosing similar complex hydro-climatic systems globally, offering a crucial scientific basis for sustainable water resource management in an era of accelerating environmental change.

~~This study developed and implemented a novel attribution framework HAAF, integrating PIML models with the Budyko framework and a lake water balance model, to quantitatively separate the impacts of climate change and human activities on the centennial hydrology of the Lake Balkhash basin. Our primary objective was to provide a comprehensive, quantitative explanation for the lake's historical water level dynamics by tracing the drivers of change from the catchment to the lake terminus. Our key findings are as follows:~~

~~(1) The HAAF successfully reconstructed the naturalized and human-impacted streamflow with high fidelity (KGE > 0.75, |PBIAS| < 10% for most stations), establishing a robust foundation for attribution analysis. The final integrated validation confirmed that our framework accurately closes the lake's water balance, with simulated volume changes strongly correlating with satellite-derived observations (R = 0.86).~~

~~(2) At the catchment scale, our attribution of runoff changes revealed a powerful dynamic of opposing forces. During the intensive intervention period (1970-1990), direct human activities were the overwhelming driver of runoff decline, causing a reduction of -9.21 km³. This immense anthropogenic pressure completely masked a significant climate-driven potential for a wetter regime (+6.13 km³). Subsequently, during the recent period (1991-2024), the basin's hydrology entered a state of fragile equilibrium, where a massive climate-driven potential for runoff increase (+10.80 km³) was almost entirely counteracted by the sustained impact of human water use (-11.36 km³).~~

~~(3) These catchment-scale dynamics directly governed the lake's response. The apparent stability of Lake Balkhash in recent decades was not a sign of resilience but was heavily subsidized by a highly favorable climatic trend that buffered the system against persistent anthropogenic water stress. However, our future projections under multiple SSP scenarios reveal that this climatic buffer is likely transient. As the favorable climatic conditions wane, the underlying pressures from human activities and cryospheric decline are projected to dominate, leading to a rapid and severe drop in the lake's water level. This demonstrates that the current equilibrium is precarious and masks a profound long-term vulnerability.~~

~~In conclusion, our research reveals that the apparent recent stability of Lake Balkhash is not a sign of systemic recovery but a fragile illusion sustained by a transient climatic boon—a state of "masked vulnerability." This study underscores the critical need for transboundary water management strategies that look beyond recent trends and account for the underlying, competing drivers of the system. The HAAF framework presented here provides a powerful tool for diagnosing similar complex hydro-climatic systems globally, offering a crucial scientific basis for sustainable water resource management in an era of accelerating environmental change.~~

Data availability. ~~All underlying data used in this research study are openly available. The sources are mentioned in Sect. 2.2. Model outputs as well as code may be made available by request to the corresponding author.~~ All underlying data used in this study are publicly accessible. The specific sources and access links are as follows: Copernicus GLO-90 DEM is available via OpenTopography (https://doi.org/10.5069/G9028PQB). DSOLMap soil properties are accessible through the WateriTech platform (https://www.wateritech.com/data). GLC_FCS30D land cover data can be downloaded from the Zenodo repository (https://zenodo.org/records/8239305). RGI v7.0 glacier data are provided by the GLIMS initiative (https://doi.org/10.5067/f6jmovy5navz). SWORD v15 hydrological networks are available at the SWOT mission river database (https://zenodo.org/records/10013982/). CRU JRA v3.0 and TerraClimate datasets are accessible via the CEDA Archive (https://catalogue.ceda.ac.uk/uuid/90a87c8fd63c4520a33445e7b6a20688/) and the Climatology Lab (https://www.climatologylab.org/), respectively. NEX-GDDP-CMIP6 projections are hosted by the NASA Earth Exchange (https://nex-gddp-cmip6.s3.us-west-2.amazonaws.com/index.html). Observed streamflow and lake level data were obtained from the National Cryosphere Desert Data Center (http://www.ncdc.ac.cn) and previously published literature (Duan et al., 2020). The model outputs and customized processing codes developed in this study are available from the corresponding author upon reasonable request.

Author contributions. Jinglu Wu designed the study. Ruibiao Yang performed the analysis and wrote the manuscript. All authors commented on the manuscript.

Competing interests. The contact author has declared that none of the authors has any competing interests.

Financial support: We thank the CAS Research Center for Ecology and Environment of Central Asia for assistance with this work. This study was supported by the National Natural Science Foundation of China (U2003202), and the Third Xinjiang Scientific Expedition and Research Program (Grant No. 2022xjkk070201).

Formatted: Font: (Default) +Headings (Times New Roman), 10 pt

Formatted: Font: (Default) +Headings (Times New Roman)

Formatted: Font: (Default) +Headings (Times New Roman)

Formatted: Font: (Default) +Headings (Times New Roman)

Formatted: Font: (Default) +Headings (Times New Roman)

Formatted: Font: (Default) +Headings (Times New Roman)

Formatted: Font: (Default) +Headings (Times New Roman)

Formatted: Font: (Default) +Headings (Times New Roman)

Formatted: Font: (Default) +Headings (Times New Roman)

Formatted: Left, Line spacing: single

Appendix A: Appendix figures

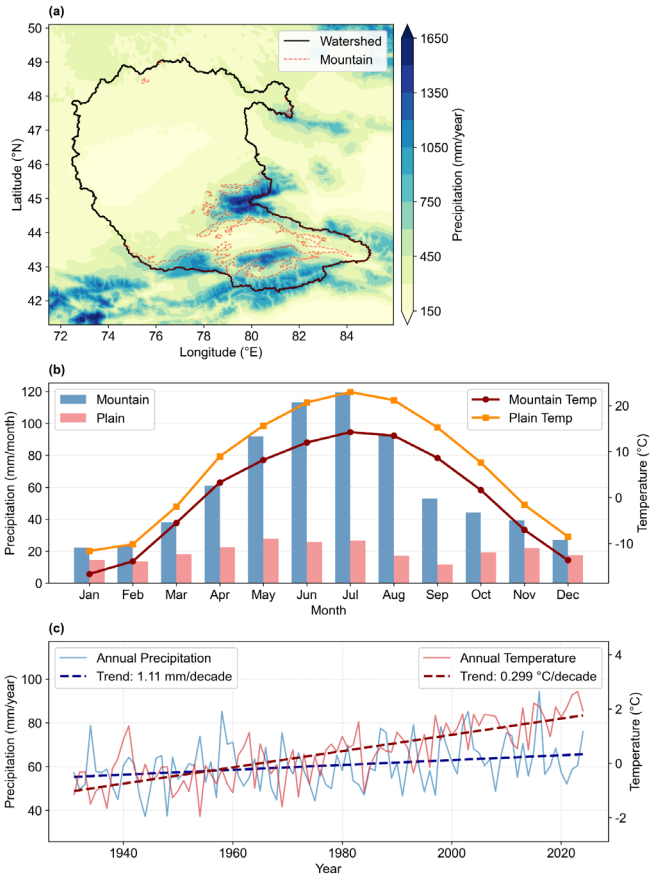

Figure A1. Spatiotemporal characteristics of climate variables in the Lake Balkhash Basin. (a) Spatial distribution of Mean Annual Precipitation (MAP) across the basin, highlighting the contrast between the mountainous upstream regions and the arid plains. (b) Seasonal cycle of monthly mean precipitation (bars, left axis) and temperature (lines, right axis), comparing the Mountainous (upstream) and Plain (downstream) regions. (c) Long-term trends in annual mean temperature and precipitation for the mountainous region from 1931 to 2024. The dashed lines represent the

Formatted: Font: (Default) +Headings (Times New Roman), Font color: Auto

Formatted: Font: (Default) +Headings (Times New Roman)

Formatted: Normal

Formatted: Font: (Default) +Headings (Times New Roman), Bold

linear trends, with statistical significance indicated in the legend. Note the accelerated warming trend observed in recent decades.

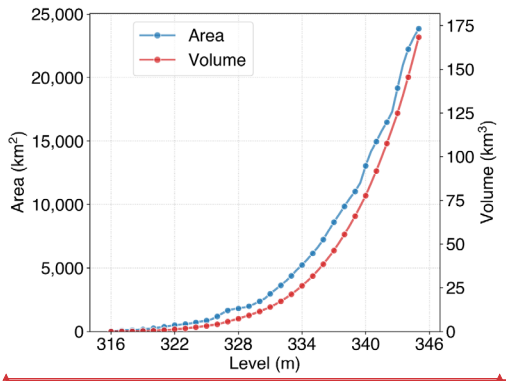

Figure A2. Stage-area and stage-volume relationships for Lake Balkhash. The blue line represents the relationship between water level and surface area (left axis), while the red line indicates the relationship between water level and storage volume (right axis). Data derived from Myrzakhmetov et al. (2022).

Formatted: Font: (Default) +Headings (Times New Roman)

Formatted: Font: (Default) +Headings (Times New Roman)

Formatted: Font: (Default) +Headings (Times New Roman)

Formatted: Font: (Default) +Headings (Times New Roman), Bold

Formatted: Font: (Default) +Headings (Times New Roman)

Appendix B: Appendix tables

Table B1. Details of the 16 hydrological stations used in this study

River System	Station Name	Longitude (°E)	Latitude (°N)	Site Elevation (m)	Drainage Area (×10^2 km^2)	Observation Period & Resolution
Ili	Ushzharma	75.83	44.93	381	1311.7	1939-1989 (monthly); 1931-2020 (yearly)
	Kapchagay	76.98	44.13	431	1141.0	1935-1989 (monthly); 1931-2000 (yearly)
	Dobyn	79.43	43.94	498	756.4	1931-2020 (yearly)
	Kairgan	80.48	43.78	529	630.6	1931-2020 (yearly)
	Yamate	81.8	43.63	692	476.2	1953-1980,2005-2008 (monthly)
	Tuohai	81.91	43.81	804	95.4	1953-1980 (monthly); 1931-2015 (yearly)
	Qiafuqihai	82.49	43.4	878	275.2	1958-1980 (monthly)
	Sliyaniya Su	79.82	44.47	1226	11.3	1936-1952, 1959-1986 (monthly)
	Sarytogay	79.22	43.51	760	77.8	1935-1989 (monthly)
	Malybay	78.4	43.43	879	42.5	1936-1989 (monthly)
Karatal	Ushtobe	77.97	45.19	422	128.0	1936-1989 (monthly)
	Tekeli	78.78	44.87	1022	11.7	1940-1955, 1959-1986 (monthly)
Aksu	Chann	79.54	45.38	667	13.4	1937-1983 (monthly)
Lepsy	Lepsy	78.33	46.28	346	101.9	1936-1989 (monthly)
	Lepsinsk	80.55	45.55	936	12.2	1931-1975 (monthly)
Ayaguz	Ayaguz	79.56	46.96	364	125.9	1949-1986 (yearly)

Table B2. Hyperparameter optimization ranges and selected values for the machine learning models

Model	Hyperparameter	Search Range	Optimal Value
ANN	Hidden Layers	[1, 2, 3]	*2*
	Neurons per Layer	[16, 32, 64, 128]	*64*
	Learning Rate	[0.001, 0.01, 0.1]	*0.01*
	Activation Function	[ReLU, Tanh, Sigmoid]	*ReLU*
LSTM	Hidden Units	[32, 64, 128, 256]	*128*
	Lookback Window	[5, 10, 15, 30] days	*15*
	Dropout Rate	[0.1, 0.2, 0.3, 0.5]	*0.2*
	Epochs	[50, 100, 200]	*100*
Random Forest	n_estimators (Trees)	[100, 300, 500, 1000]	*500*
	Max Depth	[10, 20, 30, None]	*20*
	Min Samples Split	[2, 5, 10]	*5*
XGBoost	Learning Rate (eta)	[0.01, 0.05, 0.1, 0.3]	*0.05*
	Max Depth	[3, 5, 7, 9]	*7*
	n_estimators	[100, 500, 1000]	*500*
	Subsample	[0.6, 0.8, 1.0]	*0.8*

Table B3. Performance comparison of SEGSWAT+ (Raw) and the Hybrid Model (Corrected) across calibration and validation periods

River	Station	Period	Metric	SEGSWAT+ (Raw)	Hybrid Model (Corrected)
Ili	Ushzharma	Calibration	KGE	0.68	0.89
			NSE	0.72	0.93
			PBIAS(%)	-9.5	3.2
		Validation	KGE	0.65	0.85
			NSE	0.68	0.88
			PBIAS(%)	-16.8	5.1
Karatal	Ushtobe	Calibration	KGE	0.74	0.89
			NSE	0.76	0.91
			PBIAS(%)	11.2	6.4
		Validation	KGE	0.71	0.86
			NSE	0.72	0.85
			PBIAS(%)	18.5	7.5

Aksu	Chann	Calibration	KGE	0.66	0.83
			NSE	0.64	0.84
			PBIAS(%)	-9.3	-2.8
		Validation	KGE	0.62	0.80
			NSE	0.60	0.78
			PBIAS(%)	-13.5	-3.4
Lepsy	Lepsinsk	Calibration	KGE	0.70	0.82
			NSE	0.71	0.84
			PBIAS(%)	9.8	-5.1
		Validation	KGE	0.68	0.80
			NSE	0.67	0.77
			PBIAS(%)	11.5	-6.2
Ayaguz	Ayaguz	Calibration	KGE	0.63	0.89
			NSE	0.61	0.88
			PBIAS(%)	-15.4	-0.5
		Validation	KGE	0.71	0.86
			NSE	0.68	0.83
			PBIAS(%)	-8.45	-1.8

Formatted: Font: (Default) +Headings (Times New Roman)
Formatted: Centered
Formatted: Font: (Default) +Headings (Times New Roman)
Formatted: Centered
Formatted: Font: (Default) +Headings (Times New Roman)
Formatted: Centered
Formatted: Font: (Default) +Headings (Times New Roman)
Formatted: Centered
Formatted: Font: (Default) +Headings (Times New Roman)
Formatted: Centered
Formatted: Font: (Default) +Headings (Times New Roman)
Formatted: Centered
Formatted: Font: (Default) +Headings (Times New Roman)
Formatted: Centered
Formatted: Font: (Default) +Headings (Times New Roman)
Formatted: Centered
Formatted: Font: (Default) +Headings (Times New Roman)
Formatted: Centered
Formatted: Font: (Default) +Headings (Times New Roman)
Formatted: Centered
Formatted: Font: (Default) +Headings (Times New Roman)
Formatted: Centered
Formatted: Font: (Default) +Headings (Times New Roman)
Formatted: Centered
Formatted: Font: (Default) +Headings (Times New Roman)
Formatted: Centered
Formatted: Font: (Default) +Headings (Times New Roman)
Formatted: Centered
Formatted: Font: (Default) +Headings (Times New Roman)
Formatted: Centered
Formatted: Font: (Default) +Headings (Times New Roman)
Formatted: Centered
Formatted: Font: (Default) +Headings (Times New Roman)
Formatted: Centered
Formatted: Font: (Default) +Headings (Times New Roman)
Formatted: Centered
Formatted: Font: (Default) +Headings (Times New Roman)

Appendix C: Appendix equations

C1. Estimation of Deltaic Water Consumption

According to (Xie et al., (2011), the annual water consumption in the Ili Delta (Y_i) is estimated using a multi-linear regression framework based on lake levels, river discharge, and hydro-climatic variables. The empirical equations are defined for two distinct historical periods to account for changes in the delta's eco-hydrological state:

$$Y_i = 540.5868 - 2.2890X_{i-1}^{bl} - 0.2976X_i^{be} - 0.0684X_i^{U_1} + 0.0062X_i^{U_2} + 0.0191X_i^{U_3} - 0.1496X_i^{U_4} + 0.0296X_i^{U_5} + 0.0036X_i^{U_6} + 0.0303X_i^{U_7} + 0.0308X_i^{U_8} - 0.0453X_i^{U_9} - 0.0506X_i^{U_{10}} + 0.0876X_i^{U_{11}} - 0.0051X_i^{U_{12}} + 0.2074X_i^{R} + 25.0280X_i^{T}$$

Variable Definitions and Units:

Y_i: Annual water consumption of the Ili Delta in year i ($10^8 m^3$);

X_{i-1}^{bl}: Water level of Lake Balkhash in the preceding year ($i-1$, in meters);

X_i^{be}: Total open-water evaporation of Lake Balkhash from May to September in year i ($10^8 m^3$);

$X_i^{U_1} \ldots X_i^{U_{12}}$: Monthly river discharge from January to December at the Ushzharma hydrological station in year i ($10^8 m^3$);

X_i^{R}: Total precipitation in the delta from May to August in year i (mm);

X_i^{T}: Average air temperature in the delta from May to August in year i (°C).

Formatted: Font: (Default) +Headings (Times New Roman), Font color: Auto
Formatted: Font: (Default) +Headings (Times New Roman)
Formatted: Font: (Default) +Headings (Times New Roman)
Formatted: Font: (Default) +Headings (Times New Roman)
Formatted: Font: (Default) +Headings (Times New Roman)
Formatted: Font: (Default) +Headings (Times New Roman)
Formatted: Font: (Default) +Headings (Times New Roman)
Formatted: Font: (Default) +Headings (Times New Roman), Superscript
Formatted: Font: (Default) +Headings (Times New Roman)
Formatted: Font: (Default) +Headings (Times New Roman), Superscript
Formatted: Font: (Default) +Headings (Times New Roman)
Formatted: Font: (Default) +Headings (Times New Roman)
Formatted: Font: (Default) +Headings (Times New Roman)
Formatted: Font: (Default) +Headings (Times New Roman)
Formatted: Font: (Default) +Headings (Times New Roman)
Formatted: Font: (Default) +Headings (Times New Roman)
Formatted: Font: (Default) +Headings (Times New Roman)
Formatted: Font: (Default) +Headings (Times New Roman)
Formatted: Font: (Default) +Headings (Times New Roman)
Formatted: Font: (Default) +Headings (Times New Roman)

References

Miller, B. B. and Carter, C.: The test article, J. Sci. Res., 12, 135–147, doi:10.1234/56789, 2015.

Abatzoglou, J. T., Dobrowski, S. Z., Parks, S. A., and Hegewisch, K. C.: TerraClimate, a high-resolution global dataset of monthly climate and climatic water balance from 1958–2015, Sci. Data, 5, 170191, https://doi.org/10.1038/sdata.2017.191, 2018.

Alimkulov, S., Makhmudova, L., Talipova, E., Baspakova, G., Myrzakhmetov, A., Smagulov, Z., and Zagidullina, A.: Long-term water level projections for lake balkhash using scenario-based water balance modeling under climate and socioeconomic uncertainties, Water, 17, 2021, https://doi.org/10.3390/w17132021, 2025.

Altenau, E. H., Pavelsky, T. M., Durand, M. T., Yang, X., Frasson, R. P. de M., and Bendezu, L.: The surface water and ocean topography (SWOT) mission river database (SWORD): A global river network for satellite data products, Water Resources Research, 57, e2021WR030054, https://doi.org/10.1029/2021WR030054, 2021.

Behrouz, M. S., Yazdi, M. N., and Sample, D. J.: Using random forest, a machine learning approach to predict nitrogen, phosphorus, and sediment event mean concentrations in urban runoff, J. Environ. Manage., 317, 115412, https://doi.org/10.1016/j.jenvman.2022.115412, 2022.

Budyko, M. I. and Miller, D. H.: Climate and life, 1974.

Cai, M., Yang, S., Zeng, H., Zhao, C., and Wang, S.: A distributed hydrological model driven by multi-source spatial data and its application in the ili river basin of central asia, Water Resour Manage, 28, 2851–2866, https://doi.org/10.1007/s11269-014-0641-z, 2014.

Deng, M., Wang, Z., and Wang, J.: Analysis of Balkhash Lake ecological water level evolvement and its regulation strategy, Journal of Hydraulic Engineering, 42, 403–413, 2011.

Dooge, J. C. I., Bruen, M., and Parmentier, B.: A simple model for estimating the sensitivity of runoff to long-term changes in precipitation without a change in vegetation, Advances in Water Resources, 23, 153–163, https://doi.org/10.1016/S0309-1708(99)00019-6, 1999.

Duan, W., Zou, S., Chen, Y., Nover, D., Fang, G., and Wang, Y.: Sustainable water management for cross-border resources: The balkhash lake basin of central asia, 1931–2015, J Cleaner Prod, 263, 121614, https://doi.org/10.1016/j.jclepro.2020.121614, 2020.

Duan, W., Zou, S., Chen, Y., Li, Z., and Fang, G.: Analysis of Water level changes in lake balkhash and its main influencing factors during 1879-2015, Advance in Earth Sciences, 36, 950–961, 2021.

Forgrave, R., Evenson, G. R., Golden, H. E., Christensen, J. R., Lane, C. R., Wu, Q., D'Amico, E., and Prenger, J.: Wetland-mediated nitrate reductions attenuate downstream: Insights from a modeling study, Journal of Environmental Management, 370, 122500, https://doi.org/10.1016/j.jenvman.2024.122500, 2024.

Gan, G., Wu, J., Hori, M., Fan, X., and Liu, Y.: Attribution of decadal runoff changes by considering remotely sensed snow/ice melt and actual evapotranspiration in two contrasting watersheds in the Tienshan Mountains, Journal of Hydrology, 610, 127810, https://doi.org/10.1016/j.jhydrol.2022.127810, 2022.

Guo, L., Xia, Z., Zhou, H., Huang, F., and Yan, B.: Hydrological changes of the ili river in kazakhstan and the possible causes, J Hydrol Eng, 20, 05015006, https://doi.org/10.1061/(ASCE)HE.1943-5584.0001214, 2015.

Formatted: Font: (Default) +Headings (Times New Roman), Font color: Auto

Formatted: Font: (Default) +Headings (Times New Roman)

Formatted: Font: (Default) +Headings (Times New Roman)

Guo, S., Wen, Y., Zhang, X., and Chen, H.: Monthly runoff prediction using the VMD-LSTM-Transformer hybrid model: a case study of the Miyun Reservoir in Beijing, J. Water Clim. Change, 14, 3221–3236, https://doi.org/10.2166/wcc.2023.257, 2023.

Ho, C.-C., Shih, P.-C., Chiang, L.-C., Lin, Y.-X., Liu, H.-F., Chang, W.-G., and Lin, G.-Z.: Mitigating non-point source pollution in tea plantations: SWAT modeling and field validation of slow-release fertilizers, Environ Monit Assess, 197, 810, https://doi.org/10.1007/s10661-025-14217-w, 2025.

Huang, X., Wang, Y., and Ma, X.: Simulation of extreme precipitation changes in central asia using CMIP6 under different climate scenarios, Theor Appl Climatol, 155, 3203–3219, https://doi.org/10.1007/s00704-023-04802-9, 2024.

Hugonnet, R., McNabb, R., Berthier, E., Menounos, B., Nuth, C., Girod, L., Farinotti, D., Huss, M., Dussaillant, I., Brun, F., and Kääb, A.: Accelerated global glacier mass loss in the early twenty-first century, Nature, 592, 726–731, https://doi.org/10.1038/s41586-021-03436-z, 2021.

Huss, M. and Hock, R.: Global-scale hydrological response to future glacier mass loss, Nature Clim Change, 8, 135–140, https://doi.org/10.1038/s41558-017-0049-x, 2018.

Immerzeel, W. W. and Bierkens, M. F. P.: Asia's water balance, Nature Geosci, 5, 841–842, https://doi.org/10.1038/ngeo1643, 2012.

Jackson, R., Idso, S., Reginato, R., and Pinter, P.: Canopy temperature as a crop water-stress indicator, Water Resour. Res., 17, 1133–1138, https://doi.org/10.1029/WR017i004p01133, 1981.

Jia, Q. M., Li, Y. P., Li, Y. F., and Huang, G. H.: Analyzing variation of inflow from the syr darya to the aral sea: A bayesian-neural-network-based factorial analysis method, Journal of Hydrology, 587, 124976, https://doi.org/10.1016/j.jhydrol.2020.124976, 2020.

Jin, C., Wang, B., Cheng, T. F., Dai, L., and Wang, T.: How much we know about precipitation climatology over tianshan mountains—the central asian water tower, npj Climate and Atmospheric Science, 7, 1–10, https://doi.org/10.1038/s41612-024-00572-x, 2024.

Kezer, K. and Matsuyama, H.: Decrease of river runoff in the Lake Balkhash basin in Central Asia, Hydrol Process, 20, 1407–1423, https://doi.org/10.1002/hyp.6097, 2006.

Li, J., Chen, X., Kurban, A., Van de Voorde, T., De Maeyer, P., and Zhang, C.: Identification of conservation priorities in the major basins of central asia: Using an integrated GIS-based ordered weighted averaging approach, Journal of Environmental Management, 298, 113442, https://doi.org/10.1016/j.jenvman.2021.113442, 2021.

Li, L., Long, D., Wang, Y., and Woolway, R. I.: Global dominance of seasonality in shaping lake-surface-extent dynamics, Nature, 642, 361–368, https://doi.org/10.1038/s41586-025-09046-3, 2025.

Li, Y., Chang, J., Wang, Y., Jin, W., and Guo, A.: Spatiotemporal impacts of climate, land cover change and direct human activities on runoff variations in the wei river basin, China, Water, 8, 220, https://doi.org/10.3390/w8060220, 2016.

Liu, S., Long, A., Yan, D., Luo, G., and Wang, H.: Predicting ili river streamflow change and identifying the major drivers with a novel hybrid model, J Hydrol: Reg Stud, 53, 101807, https://doi.org/10.1016/j.ejrh.2024.101807, 2024.

Lopez-Ballesteros, A., Nielsen, A., Castellanos-Osorio, G., Trolle, D., and Senent-Aparicio, J.: DSOLMap, a novel high-resolution global digital soil property map for the SWAT plus model: Development and hydrological evaluation, Catena, 231, 107339, https://doi.org/10.1016/j.catena.2023.107339, 2023.

Mandal, N. and Chanda, K.: Contribution of climate and catchment characteristics to runoff variations in Indian river basins: A climate elasticity approach, Hydrological Sciences Journal, 68, 1693–1710, https://doi.org/10.1080/02626667.2023.2236092, 2023.

Mishra, K., Choudhary, B., and Fitzsimmons, K. E.: Predicting and evaluating seasonal water turbidity in lake balkhash, kazakhstan, using remote sensing and GIS, Front. Environ. Sci., 12, https://doi.org/10.3389/fenvs.2024.1371759, 2024.

Mohammadi, B.: A review on the applications of machine learning for runoff modeling, Sustain. Water Resour. Manag., 7, 98, https://doi.org/10.1007/s40899-021-00584-y, 2021.

Myrzakhmetov, A., Dostay, Z., Alimkulov, S., Tursunova, A., and Sarsenova, I.: Level regime of balkhash lake as the indicator of the state of the environmental ecosystems of the region, Paddy Water Environ, 20, 315–323, https://doi.org/10.1007/s10333-022-00890-x, 2022.

Peng, S., Ding, Y., Liu, W., and Li, Z.: 1km monthly temperature and precipitation dataset for China from 1901 to 2017, Earth Syst. Sci. Data, 11, 1931–1946, https://doi.org/10.5194/essd-11-1931-2019, 2019.

Sánchez-Gómez, A., Bieger, K., Schürz, C., Rodríguez-Castellanos, J. M., and Molina-Navarro, E.: Multi-spatial and multi-criteria calibration to guarantee a robust SWAT+ hydrological model in a large and heterogeneous catchment, CATENA, 261, 109508, https://doi.org/10.1016/j.catena.2025.109508, 2025.

Shen, B., Wu, J., Zhan, S., Jin, M., Saparov, A. S., and Abuduwaili, J.: Spatial variations and controls on the hydrochemistry of surface waters across the ili-balkhash basin, arid central asia, Journal of Hydrology, 600, 126565, https://doi.org/10.1016/j.jhydrol.2021.126565, 2021.

Sorg, A., Bolch, T., Stoffel, M., Solomina, O., and Beniston, M.: Climate change impacts on glaciers and runoff in tien shan (central asia), Nature Clim Change, 2, 725–731, https://doi.org/10.1038/nclimate1592, 2012.

Srinivasulu, S. and Jain, A.: A comparative analysis of training methods for artificial neural network rainfall–runoff models, Appl. Soft Comput., 6, 295–306, https://doi.org/10.1016/j.asoc.2005.02.002, 2006.

Starodubtsev, V. M. and Truskavetskiy, S. R.: Desertification processes in the ili river delta under anthropogenic pressure, Water Resour, 38, 253–256, https://doi.org/10.1134/S0097807811010167, 2011.

Wang, H., Li, Y., Huang, G., Ma, Y., Zhang, Q., and Li, Y.: Analyzing variation of water inflow to inland lakes under climate change: Integrating deep learning and time series data mining, Environmental Research, 259, 119478, https://doi.org/10.1016/j.envres.2024.119478, 2024.

Wang, S. and Peng, H.: Multiple spatio-temporal scale runoff forecasting and driving mechanism exploration by K-means optimized XGBoost and SHAP, J. Hydrol., 630, 130650, https://doi.org/10.1016/j.jhydrol.2024.130650, 2024.

Wang, Z., Huang, Y., Liu, T., Zhong, R., Zan, C., and Wang, X.: Analyzing the water balance of Lake Balkhash and its influencing factors, Arid Zone Research, 39, 400–409, 2022.

Xie, L., Long, A., Deng, M., Li, X., and Wang, J.: Study on Ecological Water Consumption in Delta of the Lower Reaches of Ili River, Journal of Glaciology and Geocryology, 33, 11, 2011.

Yang, C., Xu, M., Fu, C., Kang, S., and Luo, Y.: The Coupling of Glacier Melt Module in SWAT+ Model Based on Multi-Source Remote Sensing Data: A Case Study in the Upper Yarkant River Basin, Remote Sensing, 14, 6080, https://doi.org/10.3390/rs14236080, 2022.

Yang, H., Yang, D., Lei, Z., and Sun, F.: New analytical derivation of the mean annual water-energy balance equation, Water Resources Research, 44, https://doi.org/10.1029/2007WR006135, 2008.

Yang, R., Wu, J., Gan, G., Guo, R., and Zhang, H.: Combining physical hydrological model with explainable machine learning methods to enhance water balance assessment in glacial river basins, Water, 16, 3699, https://doi.org/10.3390/w16243699, 2024.

Yu, J., Gao, B., Li, M., and Xiao, P.: Improving runoff modelling through strengthened snowmelt and glacier module enhances runoff attribution in a large watershed in central asia, Journal of Hydrology, 660, 133528, https://doi.org/10.1016/j.jhydrol.2025.133528, 2025.

Zhan, Z., Li, Z., Mu, J., Ma, H., Liang, Q., Wang, Q., Xi, H., Wang, F., Yang, Y., Zhao, W., and Lu, Z.: Glaciers and their changes based on Chinese glacier inventories in ili river basin, xinjiang, northwestern China, Research in Cold and Arid Regions, https://doi.org/10.1016/j.rcar.2025.04.001, 2025.

Zhang, G., Xie, H., Yao, T., and Kang, S.: Water balance estimates of ten greatest lakes in China using ICESat and landsat data, Chin. Sci. Bull., 58, 3815–3829, https://doi.org/10.1007/s11434-013-5818-y, 2013.

Zhang, X., Kurbaniyazov, A., and Kirillin, G.: Changing pattern of water level trends in eurasian endorheic lakes as a response to the recent climate variability, Remote Sensing, 13, 3705, https://doi.org/10.3390/rs13183705, 2021.

Zhang, X., Zhao, T., Xu, H., Liu, W., Wang, J., Chen, X., and Liu, L.: GLC_FCS30D: The first global 30 m land-cover dynamics monitoring product with a fine classification system for the period from 1985 to 2022 generated using dense-time-series landsat imagery and the continuous change-detection method, Earth System Science Data, 16, 1353–1381, https://doi.org/10.5194/essd-16-1353-2024, 2024.

Zhao, Z., Wei, F., Wu, H., Yang, M., Jin, X., Wang, P., and Wang, Q.: A framework to comprehensively assess lake health from a perspective of ecosystem integrity and services, Ecological Indicators, 171, 113169, https://doi.org/10.1016/j.ecolind.2025.113169, 2025.

Formatted: Font: (Default) +Headings (Times New Roman)